

21031
3-1-
**IMPACT DAMAGE RESISTANCE OF COMPOSITE FUSELAGE
STRUCTURE, PART I¹**

E. F. Dost, W. B. Avery, L. B. Ilcewicz, and D. H. Grande

Boeing Commercial Airplane Group, Seattle, WA.

B. R. Coxon

Integrated Technologies, Inc., Bothell, WA.

NASA
520-05
51360
P-33

ABSTRACT

Impact damage resistance of laminated composite transport aircraft fuselage structure was studied experimentally. A statistically based designed experiment was used to examine numerous material, laminate, structural, and extrinsic (e.g., impactor type) variables. The relative importance and a quantitative measure of the effect of each variable and variable interactions on responses including impactor dynamic response, visibility, and internal damage state were determined. The study utilized 32 three-stiffener panels, each with a unique combination of material type, material form, and structural geometry. Two manufacturing techniques, tow placement and tape lamination, were used to build panels representative of potential fuselage crown, keel, and lower side-panel designs. Various combinations of impactor variables representing various foreign-object-impact threats to the aircraft were examined. Impacts performed at different structural locations within each panel (e.g., skin midbay, stiffener attaching flange, etc.) were considered separate parallel experiments. The relationship between input variables, measured damage states, and structural response to this damage are presented including recommendations for materials and impact test methods for fuselage structure.

INTRODUCTION

Carbon fiber composites have the potential of reducing both the weight and cost of primary aircraft structure. The high specific stiffness and strength along with corrosion and fatigue resistance have been cited by many researchers as benefits of composite materials. One major weakness of laminated composites is their reduced strength when subject to foreign object impact. This susceptibility to impact damage has been studied by many investigators. Impact induced matrix damage has been found to reduce the compressive strength [1, 2], while fiber damage reduces both the compressive and tension strengths [3, 4].

Impact studies conducted by NASA and other researchers in the past [e.g., 1, 2, 5-7] concentrated on wing type structure. Impact testing was performed on both coupons and subcomponents using simulated impact threats, usually with a hemispherical tip. Internal Boeing studies involving various shop tools dropped onto test articles were correlated to these assumed impact threats. The coupons and subcomponents were then tested in axial compression (to simulate upper wing surface loads) to determine the effect of the damage.

¹ This work was funded by Contract NAS1-18889, under direction of J.G. Davis and W.T. Freeman of NASA Langley Research Center.

The damage states and residual strengths observed in these early tests were found to be a strong function of impact energy and relatively independent of the impactor shape. Matrix damage (i.e., delaminations and transverse cracks) was found to be the primary failure mechanism for the "brittle" epoxy laminates under study at that time. The areal extent of the matrix damage was a strong function of the impact energy. Local fiber failures were suppressed by the formation of large delaminations which reduced local contact forces by locally softening the laminate. Matrix damage dominated compression-after-impact (CAI) strength [6], while fiber failure, which would be strongly influenced by impactor geometry, was not found to be a strong contributor to the observed compression strength degradation. These findings along with ease of analytical modeling lead to the use of spherically shaped impactors with diameters between 12.7 mm and 25.4 mm for the majority of studies on impact on fibrous composites to date.

Coupon level tests such as the 6.35 mm thick NASA ST-1 [8] and the 4.6 mm thick Boeing 4"x6" CAI [6] were developed based on results and observations from these early impact studies. The design of these specimens and tests emphasized the effects of matrix damage. Much of recent composite material development efforts have concentrated on improving CAI while keeping some minimum hot/wet compression strength. Approaches for improving CAI have included toughened (high elongation) thermoset matrices [9], addition of discrete interlayers (e.g., adhesive or elastomeric particle) [10, 11], through-thickness stitching [12, 13], and braided fiber architectures [14].

Improvements in CAI by the first and second methods stated above have been accomplished by reducing the areal extent of matrix damage [15]. This reduction of delamination planar area would tend to increase local contact forces during an impact event. Braided composites may absorb some energy through matrix cracking, but delamination is suppressed by the fiber architecture [14]. Both may have a stronger tendency toward fiber failures under the impactor and have post-impact strengths influenced by impactor geometry.

An experimental study to investigate impact damage that may occur in laminated composite aircraft fuselage structure was performed. Material, laminate, structural, and numerous impact variables were considered. A design of experiments (DOE) technique was used to study the large number of variables. The relative importance and a quantitative measure of the effect of variables and variable interactions with respect to specific responses were determined. The current study utilized 32 three-stiffener panels, each with a distinct combination of material type, material form, and structural geometry to study the impact damage resistance of fuselage structure. Laminate and structural variable levels were representative of potential fuselage crown, keel, and lower side-panel designs.

TEST MATRIX DEVELOPMENT

Variable Identification

Intrinsic Variables. Aircraft fuselage can be designed with many different combinations of material, layup, and structural geometry depending on specific requirements. An aircraft fuselage may be considered as four separate quadrants, each having different design drivers. The crown (top) is dominated by tension loads, the keel (bottom) is predominantly designed by compression, and the side panels have combined shear and axial loads. The entire fuselage cylinder is subjected to hoop tension from internal pressure. An aircraft designer must choose specific values (levels) from each potential variable (e.g., fiber/matrix type, stiffener geometry, skin thickness/layup, etc.) to design the structure in each quadrant. The variables associated with the structure are termed *intrinsic* variables. Table 1 lists all intrinsic variables studied along with their respective levels.

Variable	Low Level	High Level
Fiber Type	AS4	IM7
Matrix Type	938	977-2
Fiber Volume	48%	56.5%
Material Form (Stiffener Layup)	Tow (Soft)	Tape (Hard)
Skin Layup	Soft	Hard
Stiffener Type	Blade	Hat
Stiffener Spacing	17.8 cm (7 in)	30.5 cm (12 in)
Laminate Thickness	2.26 mm (0.0888 in)	4.51 mm (0.1776 in)

Layups	
Hard Skin (Thin)	(45/ 90/ -45/ 0/ 90/ 0) _S
Soft Skin (Thin)	(45/ 90/ -45/ 45/ 0/ -45) _S
Hard Skin (Thick)	(45/ 90/ -45/ 0/ 45/ 90/ -45/ 0/ 90/ 0/ 90/ 0) _S
Soft Skin (Thick)	(45/ 90/ -45/ 45/ 0/ -45/ -45/ 0/ 45/ -45/ 90/ 45) _S
Hard Stiffener (Thin)	(22.5/ 90/ -22.5/ 0) _S
Soft Stiffener (Thin)	(30/ 90/ -30/ 0) _S
Hard Stiffener (Thick)	(22.5/ 90/ -22.5/ 0) _{2S}
Soft Stiffener (Thick)	(30/ 90/ -30/ 0) _{2S}

Table 1: Intrinsic Variables

Material variables may include fiber, matrix, and their combined architecture. Graphite or carbon fiber properties may be quantified in terms of axial stiffness, tensile strength, and cross-sectional size/shape. The matrix is generally classified by its stiffness, strengths, and in-situ composite toughness (i.e., inter- and intra-laminar toughness). The performance of the composite is influenced by the fiber/matrix architecture. This is characterized by the overall fiber volume, fiber/resin distribution, interlayer structure, amount of fiber waviness, void content, and fiber-matrix interface. Many of these material attributes are not controllable when two or more of are studied simultaneously. Variables considered for study were fiber type, matrix type, and overall fiber volume.

Various schemes for manufacturing laminates exist, including hand layup, automatic tape layup (ATL), filament winding, advanced tow placement (ATP), and resin transfer molding (RTM). Cost effective fabrication of large fuselage quadrants requires lamination flexibility including the ability to tailor thickness and follow surfaces with complex contours. Hand layup and ATP were chosen for this study because both meet these lamination flexibility requirements. In addition, hand layup offers a well understood material form and part performance, while ATP offers reduced manufacturing and raw material costs. Laminate layup and thickness were also included as variables in these experiments.

Structural configuration has a strong influence on the cost, weight, and assembly of the fuselage [16]. Structural performance; including local skin buckling, overall panel stability, impact damage resistance, and damage tolerance, is governed by the skin thickness and stiffness; stiffener geometry, layup, and spacing; and the applied loads. Blade and closed hat stiffeners were studied because they provide a distinct range in structural response for stiffened-skin panel construction.

Extrinsic Variables. The potential for foreign-object impact on aircraft primary structure starts the day the first element is cured and continues until the aircraft is retired from service. Threats include

dropped hand and power tools, tool boxes, hail, runway debris, engine-burst fragments, ground handling equipment [17]. Generally, impacts may occur at any location on both the inner and outer surfaces of the structure, although certain types of impacts will be constrained to specific regions of the aircraft (e.g., hail will generally strike the crown, other horizontal surfaces, leading edges, and nose of the aircraft). The environment during an impact event is governed by those the aircraft may see while in service. Variables associated with an impact event including when, how, and where, are classified as *extrinsic* variables.

Impact threats may be categorized by the mass, shape, size, stiffness, velocity, and incidence angle of the impactor. The current experiment considered all of these impactor variables, except incidence angle and velocity. Impacting at oblique angles was found to be experimentally difficult with the equipment available. Impact energy was substituted for impact velocity because unrealistically high impact energies result when velocity and mass are combined in a partially crossed experiment. Temperature at impact was chosen to examine the effect of environment on impact damage. All extrinsic variables and the associated levels are listed in Table 2.

Variable	Low Level	High Level
Impactor Stiffness	2.8 GPa (0.4 Msi)	210 GPa (30 Msi)
Impactor Mass	0.28 kg (0.62 lbm)	6.31 kg (13.9 lbm)
Impact Energy	23 J (200 in-lb)	136 J (1200 in-lb)
Impactor Shape	Flat	Spherical
Impactor Diameter	6.35 mm (0.25 in)	25.4 mm (1.00 in)
Temperature at Impact	21°C (70°F)	83°C (180°F)

Table 2: Extrinsic Variables

Design of Experiments. The final experiment examined fourteen variables to determine their relationship to fuselage impact damage resistance. The examination of this large number of variables within one comprehensive study required the use of a statistical technique known as *Design of Experiments (DOE)* [18, 19]. A DOE provides a systematic way to design an efficient experiment, collect data, and analyze the results. The DOE used for this study, a 32 run, split-plot fractional factorial design, provided information on the main variables and indicated whether variable interactions existed.

The use of this DOE put limitations on the number of variable levels and the types of variables which could be studied. The number of variable levels was restricted to two, and had to be chosen so that unrealistic combinations were avoided, yet were representative of potential fuselage designs. Decisions on conflicting variables were made based on practical considerations and our knowledge and intuition of impact damage resistance. Table 3 contains a list of the variables studied with their respective levels as they fit into the DOE.

The design of experiments technique required quantifiable response measurements for all 32 runs to evaluate the effect of variables and interactions. Responses measured and studied via the DOE included: indentation depth, planar damage area, and fiber damage average length and through-thickness distribution. Preliminary results of flexural wave propagation measurements are presented, but not analyzed in the context of the DOE.

Table 3: Thirty-Two DOE Runs with Variable Levels

Run #	Panel ID	Fiber Type	Matrix Type	Fiber Volume	Material Form (Stiffener Layout)	Skin Layup	Stiffener Type	Stiffener Web Spacing	Laminates Thickness	Impactor Stiffness	Impact Mass	Impact Energy	Impactor Shape	Impactor Diameter	Temperature
1	28-1B	AS4	938	0.480	Tow (Soft)	Soft	Blade	17.8 cm	2.26 mm	3 GPa	0.28 kg	23 J	Flat	6.35 mm	210C
2	28-1A	AS4	938	0.480	Tow (Soft)	Soft	Blade	17.8 cm	4.51 mm	3 GPa	6.31 kg	136 J	Spherical	25.4 mm	830C
3	29-7A	AS4	938	0.480	Tow (Soft)	Hard	Hat	30.5 cm	4.51 mm	210 GPa	6.31 kg	136 J	Flat	6.35 mm	210C
4	29-7B	AS4	938	0.480	Tape (Hard)	Hard	Hat	30.5 cm	2.26 mm	210 GPa	0.28 kg	23 J	Spherical	25.4 mm	830C
5	28-2B	AS4	938	0.565	Tape (Hard)	Hard	Blade	17.8 cm	2.26 mm	210 GPa	0.28 kg	136 J	Spherical	25.4 mm	210C
6	28-2A	AS4	938	0.565	Tape (Hard)	Soft	Blade	17.8 cm	4.51 mm	210 GPa	6.31 kg	23 J	Flat	6.35 mm	830C
7	28-6A	AS4	938	0.565	Tape (Hard)	Soft	Hat	30.5 cm	2.26 mm	3 GPa	0.28 kg	136 J	Flat	6.35 mm	210C
8	28-6B	AS4	977-2	0.565	Tape (Soft)	Soft	Hat	30.5 cm	2.26 mm	210 GPa	6.31 kg	136 J	Flat	25.4 mm	830C
9	29-7B	AS4	977-2	0.565	Tow (Soft)	Soft	Hat	17.8 cm	4.51 mm	210 GPa	0.28 kg	23 J	Spherical	25.4 mm	210C
10	29-7A	AS4	977-2	0.565	Tow (Soft)	Hard	Blade	30.5 cm	2.26 mm	3 GPa	6.31 kg	136 J	Spherical	25.4 mm	830C
11	28-7A	AS4	977-2	0.565	Tow (Soft)	Hard	Blade	30.5 cm	2.26 mm	3 GPa	0.28 kg	23 J	Spherical	25.4 mm	210C
12	28-7B	AS4	977-2	0.565	Tow (Soft)	Hard	Blade	30.5 cm	4.51 mm	3 GPa	6.31 kg	136 J	Spherical	25.4 mm	830C
13	29-2B	AS4	977-2	0.480	Tape (Hard)	Hard	Hat	17.8 cm	2.26 mm	3 GPa	0.28 kg	23 J	Spherical	25.4 mm	210C
14	29-2A	AS4	977-2	0.480	Tape (Hard)	Hard	Hat	17.8 cm	4.51 mm	210 GPa	6.31 kg	136 J	Spherical	25.4 mm	830C
15	28-8A	AS4	977-2	0.480	Tape (Hard)	Soft	Blade	30.3 cm	2.26 mm	210 GPa	0.28 kg	136 J	Flat	6.35 mm	210C
16	28-8B	AS4	977-2	0.480	Tape (Hard)	Soft	Blade	30.3 cm	4.51 mm	210 GPa	6.31 kg	23 J	Flat	25.4 mm	830C
17	29-5B	IM7	977-2	0.480	Tow (Soft)	Soft	Hat	30.3 cm	2.26 mm	3 GPa	0.28 kg	136 J	Spherical	25.4 mm	210C
18	29-5A	IM7	977-2	0.480	Tow (Soft)	Hard	Blade	17.8 cm	4.51 mm	210 GPa	6.31 kg	23 J	Spherical	25.4 mm	830C
19	28-3A	IM7	977-2	0.480	Tow (Soft)	Hard	Blade	17.8 cm	2.26 mm	210 GPa	0.28 kg	136 J	Flat	6.35 mm	210C
20	28-3B	IM7	977-2	0.480	Tape (Hard)	Hard	Blade	30.5 cm	2.26 mm	210 GPa	0.28 kg	23 J	Flat	6.35 mm	830C
21	29-6B	IM7	977-2	0.565	Tape (Hard)	Hard	Hat	30.3 cm	4.51 mm	3 GPa	6.31 kg	136 J	Spherical	25.4 mm	210C
22	29-6A	IM7	977-2	0.565	Tape (Hard)	Soft	Blade	17.8 cm	2.26 mm	210 GPa	0.28 kg	136 J	Flat	6.35 mm	830C
23	28-4B	IM7	977-2	0.565	Tape (Hard)	Soft	Blade	30.5 cm	4.51 mm	3 GPa	6.31 kg	23 J	Spherical	25.4 mm	830C
24	28-4A	IM7	977-2	0.565	Tape (Soft)	Soft	Blade	30.5 cm	2.26 mm	210 GPa	0.28 kg	136 J	Flat	6.35 mm	210C
25	28-5B	IM7	938	0.565	Tow (Soft)	Soft	Blade	17.8 cm	4.51 mm	210 GPa	0.28 kg	136 J	Spherical	25.4 mm	830C
26	28-5A	IM7	938	0.565	Tow (Soft)	Hard	Hat	30.5 cm	2.26 mm	3 GPa	6.31 kg	23 J	Flat	6.35 mm	210C
27	28-7A	IM7	938	0.565	Tow (Soft)	Hard	Hat	17.8 cm	4.51 mm	210 GPa	0.28 kg	136 J	Spherical	25.4 mm	830C
28	28-2B	IM7	938	0.480	Tape (Hard)	Hard	Blade	30.5 cm	2.26 mm	3 GPa	6.31 kg	23 J	Flat	25.4 mm	210C
29	28-6B	IM7	938	0.480	Tape (Hard)	Hard	Blade	17.8 cm	4.51 mm	210 GPa	0.28 kg	136 J	Spherical	25.4 mm	830C
30	28-6A	IM7	938	0.480	Tape (Hard)	Soft	Blade	30.3 cm	2.26 mm	210 GPa	0.28 kg	23 J	Flat	6.35 mm	210C
31	28-8A	IM7	938	0.480	Tape (Hard)	Soft	Hat	17.8 cm	4.51 mm	210 GPa	0.28 kg	23 J	Spherical	25.4 mm	830C
32	29-4B	IM7	938	0.480	Tape (Hard)	Soft	Hat	17.8 cm	2.26 mm	210 GPa	6.31 kg	136 J	Spherical	6.35 mm	210C

EXPERIMENTAL TECHNIQUE

Specimen Preparation

The intrinsic variables in the test matrix were implemented in 32 three-stiffener panels, one for each of the 32 runs of the DOE test matrix and each having a distinct combination of variable levels. Careful placement of variables into the DOE test matrix resulted in identical panel configurations except for laminate thickness for every two runs (e.g., 1 & 2, 3 & 4). Sixteen 2.79 meter long panels with a 1.27 meter long thick constant gage section, a 0.25 meter long thickness transition zone, and a 1.27 meter long thin constant gage section were designed. Formal drawings of these 16 panels were created, describing all material and fabrication requirements. An abbreviation of the drawing number followed by an "A" for the thick section and a "B" for the thin section was used to identify each panel as shown in Table 3.

Materials. Eight distinct combinations of fiber type, matrix type, fiber volume, and material form were specified by the implementation of these variables into the DOE matrix. All eight materials, four pre-impregnated tow and four pre-impregnated tape, were manufactured by ICI Fiberite. The tow was made using solvent impregnation, while tape was created using hot-melt impregnation. Minimum property requirements for acceptance tests were established from known fiber and matrix properties using micromechanics [20]. The material constitutive properties along with calculated lamina properties are given in Table 4.

Tape Hand Layup. Panels fabricated using prepreg tape hand layup were manufactured at Boeing's composite fabrication facility in Auburn, Washington. Individual plies were laminated into flat skin panels and stiffener charges using a ply layup template (PLT) created from the formal drawings. Skin and stiffener layups were vacuum compacted following application of every ply. Skin panels were stored under vacuum, while the stiffeners were being prepared.

The flat stiffener charges were formed into appropriate stiffener cross-sections following layup. Closed-hat stiffeners were formed to their final shape using one forming operation over elastomeric mandrels (Figure 1). Blade stiffeners required four major fabrication steps: first, angles were formed over polished-steel-angle mandrels; second, the angles were assembled into a blade section; third, a radius filler was formed from the pre-impregnated graphite; and fourth, the radius filler was placed into the blade between the two angles (Figure 2). The stiffeners were assembled to the skin panel per PLT markings and the assembled panel was bagged and cured per Boeing specifications.

The panel periphery and blade stiffener tops were trimmed to their final dimensions following cure. The 2.79 meter long panels were machined into the three sections described above. All panels were non-destructively inspected using 10 MHz pulse-echo ultrasonics for the skins and 5 MHz through-transmission ultrasonics for the stiffeners. The trimmed panel ends were polished and the cross-section inspected via optical microscopy to validate the ultrasound results.

MATERIAL SYSTEM	AS4/3501-6 (6k tow)	AS4/3501-6 (tape)	IM7/977-2 (12k tow)	IM7/977-2 (tape)	IM7/3501-6 (12k tow)	IM7/3501-6 (tape)	AS4/977-2 (6k tow)	AS4/977-2 (tape)
R.C.	44.4%	35.7%	44.8%	36.8%	34.9%	44.1%	37.3%	44.9%
F.V.	48.5%	56.8%	47.1%	56.3%	57.4%	48.8%	55.8%	47.3%
CONSTITUTIVE PROPS.								
fiber:								
E(1)t	3.400E+07	3.400E+07	3.800E+07	3.800E+07	3.800E+07	3.800E+07	3.400E+07	3.400E+07
E(1)c	3.250E+07	3.250E+07	3.450E+07	3.450E+07	3.450E+07	3.450E+07	3.250E+07	3.250E+07
E(2)	2.300E+06	2.300E+06	2.300E+06	2.300E+06	2.300E+06	2.300E+06	2.300E+06	2.300E+06
G(12)	2.700E+06	2.700E+06	2.600E+06	2.600E+06	2.600E+06	2.600E+06	2.700E+06	2.700E+06
NU(12)	0.300	0.300	0.310	0.310	0.310	0.310	0.300	0.300
alpha(1)	-2.000E-07	-2.000E-07	-5.100E-07	-5.100E-07	-5.100E-07	-5.100E-07	-2.000E-07	-2.000E-07
alpha(2)	5.000E-06	5.000E-06	5.200E-06	5.200E-06	5.200E-06	5.200E-06	5.000E-06	5.000E-06
density	1.73	1.78	1.80	1.73	1.80	1.73	1.73	1.78
matrix:								
E	6.200E+05	6.200E+05	5.200E+05	5.200E+05	6.200E+05	6.200E+05	5.200E+05	5.200E+05
G	2.200E+05	2.200E+05	1.800E+05	1.800E+05	2.200E+05	2.200E+05	1.800E+05	1.800E+05
NU	0.350	0.350	0.410	0.410	0.350	0.350	0.410	0.410
alpha	2.630E-05	2.630E-05	2.470E-05	2.470E-05	2.630E-05	2.630E-05	2.470E-05	2.470E-05
density	1.30	1.30	1.30	1.30	1.30	1.30	1.30	1.30
LAMINA PROPERTIES								
E(1)t	1.680E+07	1.958E+07	1.817E+07	2.164E+07	2.207E+07	1.886E+07	1.921E+07	1.634E+07
E(1)c	1.608E+07	1.873E+07	1.652E+07	1.966E+07	2.007E+07	1.715E+07	1.837E+07	1.564E+07
E(2)	1.262E+06	1.379E+06	1.109E+06	1.241E+06	1.388E+06	1.266E+06	1.233E+06	1.111E+06
G(12)	6.103E+05	7.150E+05	4.982E+05	5.973E+05	7.178E+05	6.100E+05	5.946E+05	5.023E+05
NU(12)	0.326	0.322	0.363	0.354	0.327	0.330	0.349	0.358
alpha(1)	3.266E-07	1.788E-07	-9.011E-08	-2.190E-07	-1.571E-07	-1.354E-08	1.115E-07	2.367E-07
alpha(2)	1.421E-05	1.248E-05	1.444E-05	1.256E-05	1.252E-05	1.429E-05	1.251E-05	1.427E-05

Units: Moduli in psi, Densities in kg/m³, CTE's per degree F

Room Temperature Properties

Table 4: Micromechanics Based Ply Properties

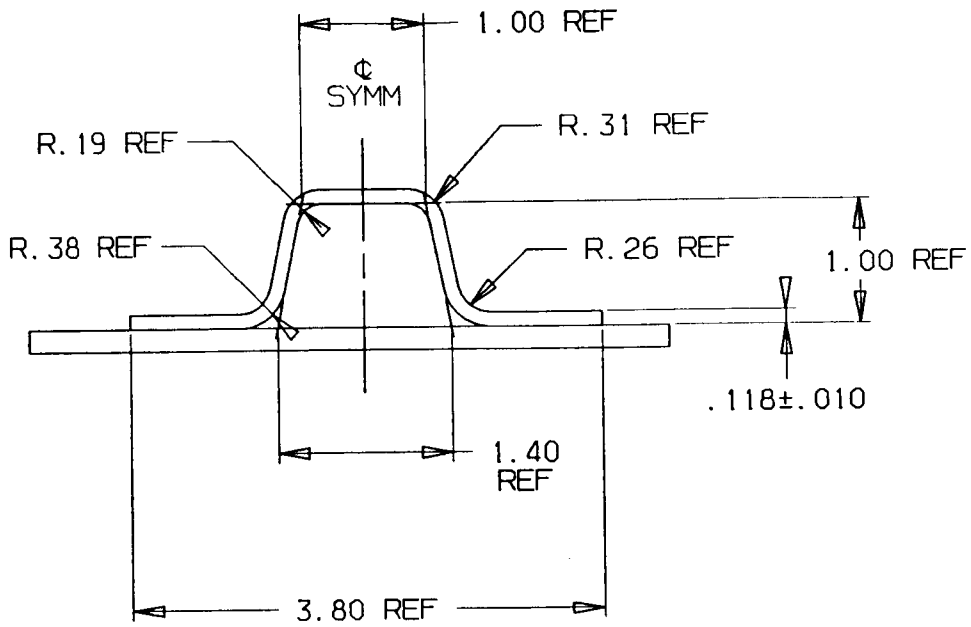


Figure 1: Thick Hat Stiffener Geometry

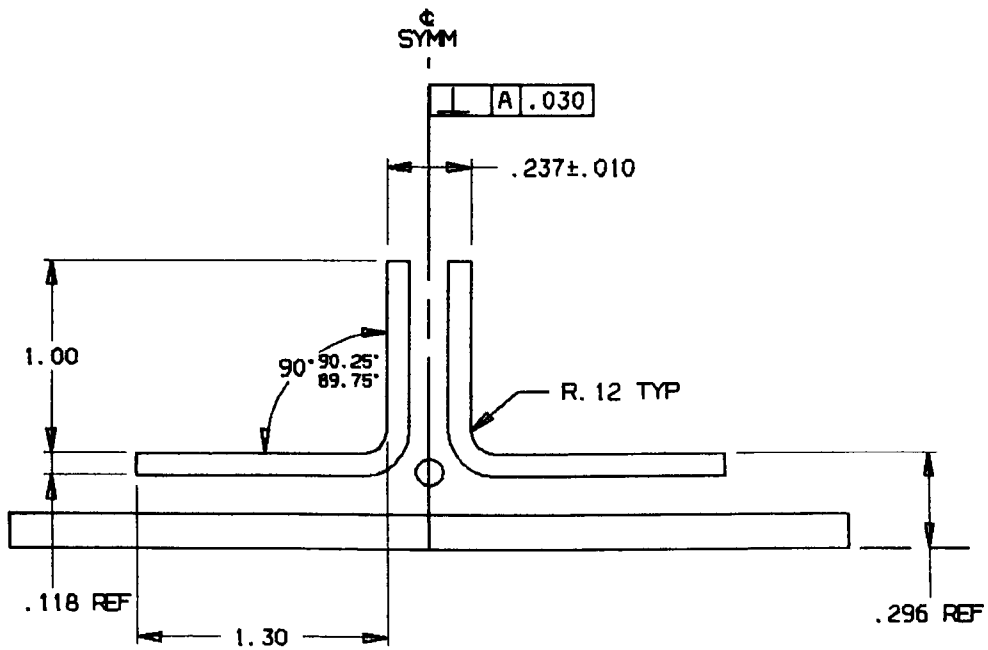


Figure 2: Thick Blade Stiffener Geometry

Tow Placement. Panels manufactured using advanced tow placement were fabricated by Hercules Incorporated's Composite Products Group. A seven-axis numerically-controlled robot was used to fabricate flat skin and stiffener charges from pre-impregnated tow. This machine collimated and spread twelve individual tows into 25 mm wide bands of the appropriate thickness. Pressure applied by the cylindrical-rolling applicator of the tow-placement head helped to compact the laminate. Additionally, the laminate was vacuum compacted following application of every fourth ply. Stiffener forming, panel assembly, bagging, and cure procedures used by Hercules were identical to those performed by Boeing.

Impact Testing

Impact testing was divided into two portions; high mass (6.31 kg) impacts and low mass (0.28 kg) impacts. The equipment used to perform these two types of impacts were of differing design. Nominally, ten impacts were performed on each panel, eight of which were based on the extrinsic variables listed in Table 2. Two additional impacts, one on the skin midbay and one over the stiffener centerline, were performed using a 63.5 mm (2.5 in) diameter lead ball dropped at 56.5 Joules (500 in-lb) to simulate 63.5 mm diameter hail at terminal velocity.

Boundary Conditions. The boundary conditions applied to all panels were designed to simulate the circumferential frames found in aircraft fuselage. Supports were placed with a span of 0.51 meter between their inner edges to simulate the fuselage 0.56 meter (22 in) centerline to centerline frame spacing. Three sets of 44.5 mm by 89.9 mm (2" X 4") fir boards were notched to provide clearance for the three stiffeners. The boards were shaved slightly at the stiffener attaching flange locations so that both the skin and attaching flanges were supported during impact. Unnotched boards were placed over the skin side and bolted to the opposing notched board to restrict panel z-axis motion.

Impacts were performed 76.2 mm (3 in) from a support. This distance allowed clearance for the impactor and was probably close to the worst case location. Additionally, it allowed maximum post-impact test of these panels by minimizing the area of panel affected by impact damage. The free end of the panel was restrained with a third pair of supports.

The panel with simulated frames was held in place by steel fixtures which were solidly mounted to cement floors. Figure 3 shows the general fixture configuration of the high mass support fixture. The low mass panel support fixture held panels vertically and is shown in Figure 4. Impact alignment was achieved by aligning crosshairs marked at the desired impact location on the panel with a pointed alignment tup mounted in the impactor. The panel was clamped in place when alignment was within ± 1.27 mm.

Impact Tups. The implementation of impactor variables into the DOE defined eight different impact tups. Materials used to fabricate these tups were steel for hard impactors and graphite/epoxy cut transverse to the plane of lamination for soft impactors. All low and high mass impactor tups were designed with sufficient length to allow panel perforation under maximum deflection.

Steel impacting tups for the high mass impactor were manufactured out of A2 steel and machined to dimensional tolerance of ± 0.051 mm and a mass of 226.8 ± 9.1 grams. The low mass impactor steel tups were machined from 4140 steel with a dimensional tolerance of ± 0.051 mm and a mass of 35.2 ± 0.2 grams. All steel tups were hardened to 55-60 Rockwell C.

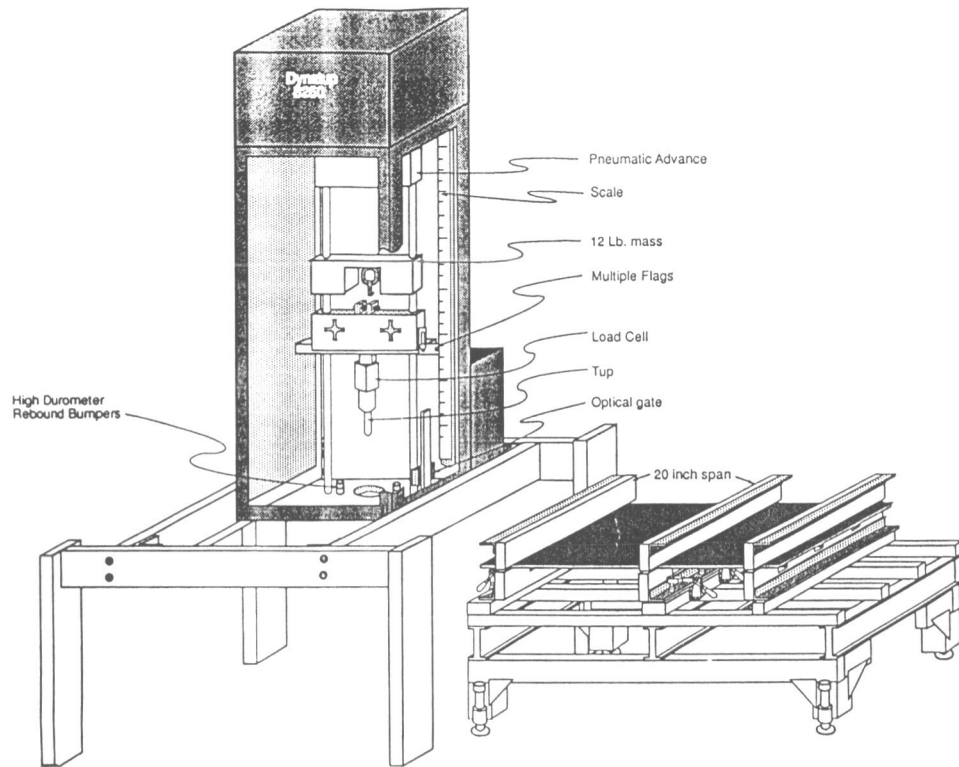


Figure 3: High Mass (Dynatup) Impact Apparatus

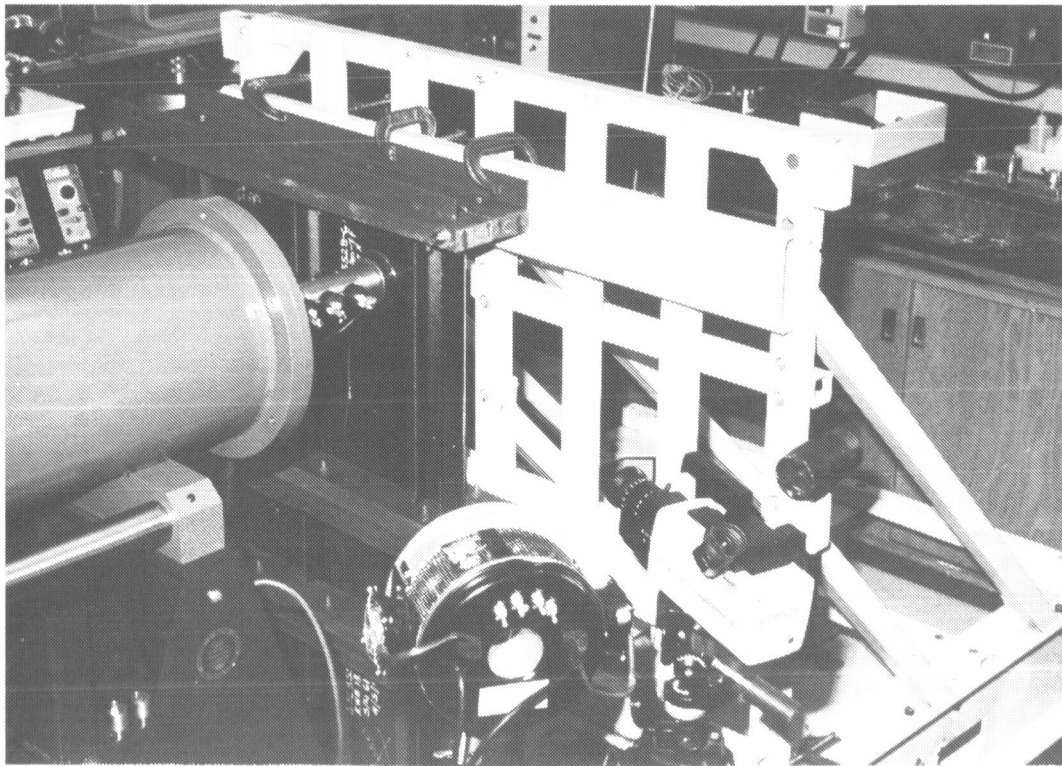


Figure 4: Low Mass (University of British Columbia) Impact Apparatus

Graphite tups were rough cut, using a waterjet cutter, from a 31.75 mm thick block of tool grade graphite-epoxy (Toolrite MXG-7650 style 2577). The 25.4 mm tups were machined to a tolerance of ± 0.76 mm in diameter. Tolerances for these graphite tups were less strict due to difficulty in lathe cutting a hemisphere without chipping or scarring the graphite/epoxy. The 6.35 mm tups were ground rather than lathe cut because of their tendency to break under lateral load. Grinding yielded tolerances of ± 0.051 mm.

Low Mass Impacts. Low mass impacts were performed at the University of British Columbia, using a horizontally oriented nitrogen gas gun. The projectile consisted of the steel or graphite tip, an aluminum shaft, a PCB 208M88 5 kip load cell, and a torlon shell as shown in Figure 5. The load cell was connected through a trailing wire to a Tektronix 2230, 100 MHz, 8 bit digital storage oscilloscope capable of storing 4096 points of data. Impact and rebound velocities were computed using three pairs of optical gates placed just before the point of impact. Data acquisition was triggered by the last optical gate with an experimentally calibrated electronic time delay circuit to assure data collection started just prior to contact. Impact velocity was calibrated as a function of firing pressure.

The impact tups were created with sufficient length to allow full penetration during impact including an allowance for panel deflection. The larger diameter backup structure was prevented from striking the panel by placing an elastomeric-ring bumper in the end of the air-gun barrel. Each panel was then carefully placed a specified distance from the end of the barrel. Secondary impacts were prevented by activating a pressure release valve which vented barrel after the gun was fired. This prevented back pressure from forcing the rebounding tup into the panel.

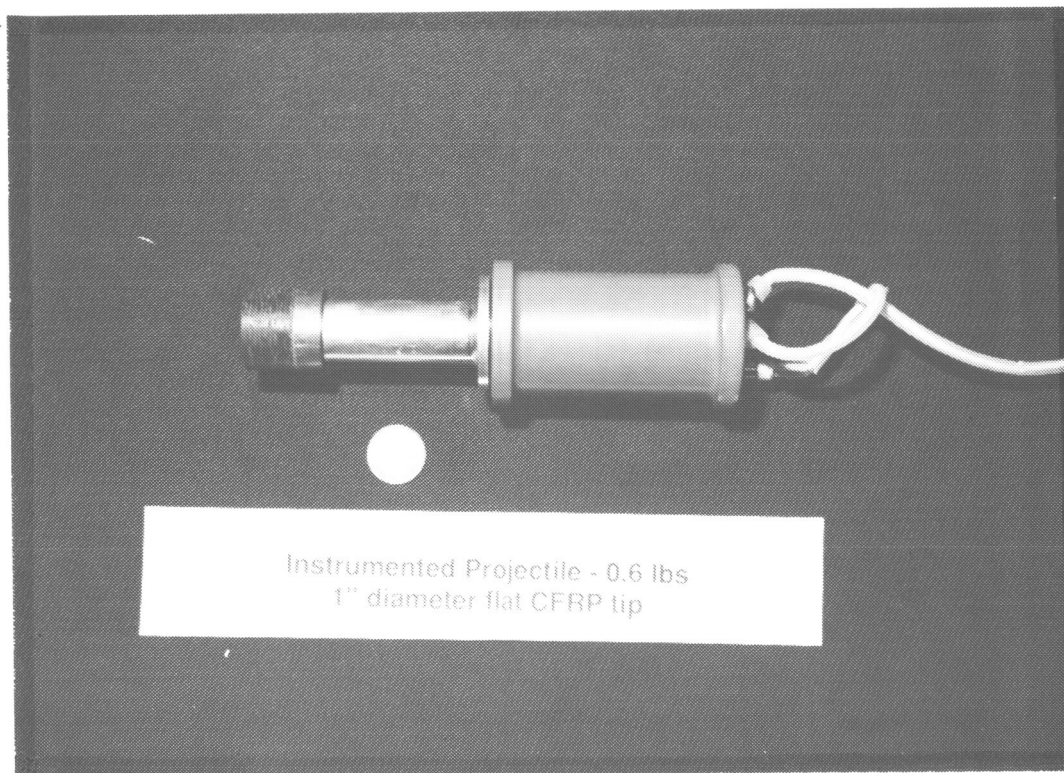


Figure 5: Low-mass Impact Projectile

High Mass Impacts. High mass impacts were performed on the Dynatup 8250 drop weight impactor schematically shown in Figure 3. Data acquisition was accomplished using a Macintosh IIcx computer equipped with a National Instruments model A2000 high speed data acquisition board operating at 500 kHz and Integrated Technologies, Inc. proprietary software. A Dynatup 10 kip load cell was conditioned using a Measurements Group 2210A signal conditioner. The range of the load cell could be changed from 44.5 MN to 22.25 MN (10 kips to 5 kips) to improve resolution using the appropriate gain settings. Impact and rebound velocities were computed using a precision machined flag which passed through an optical gate placed just before the point of impact.

Impact velocities for low energy impacts of 11.3 J (100 in-lb) to 56.5 J (500 in-lb) on the Dynatup 8250 impactor were generated by setting the impactor at an initial height, (h) and using gravitational acceleration (g) to achieve the desired energy, (E). The value of (h) was back calculated using the potential energy equation:

$$E = mgh$$

where m is the mass of the impactor. High energy impacts (< 56.5 J), which could not be achieved by gravity drops, were generated by a calibrated pneumatic system which compressed springs against the impactor. The springs imparted an initial velocity to the impacting mass when released.

High durometer elastomeric rebound bumpers were placed at a specified height to stop the impactor following perforation of a panel. The constant diameter portion of the tup was long enough to allow full penetration into the panel, again, including an allowance for panel deflection. Secondary impacts were prevented by a ratchet device which was triggered on the first pass of the impactor. This device stopped the impactor on its second pass through following rebound.

Hail Simulation. An experiment to study damage created by 63.5 mm (2.5 in) hail was performed in parallel with the full experiment. Hail of this size at terminal velocity has 500 in-lb of energy. A 63.5 mm lead ball was dropped from 3.43 meters to achieve an equivalent energy. Impacting the desired location was accomplished by aligning the base of a 76.2 mm diameter PVC tube with the impact site. The lead ball was dropped inside the tube to impact the panel. A rubber lined aluminum plate was placed between the tube and panel immediately after impact to catch the lead ball and prevent a second impact. Lead ball impacts were not instrumented and were performed at ambient temperature.

Damage Characterization

The fundamental understanding between the variables studied and resulting impact damage is accomplished by comparing measured responses. Many responses may be associated with a given impact event, including measures of the dynamic event, damage area, fiber breakage, and strength-after-impact. These responses may be broken into two major categories: discrete measurements which quantify details of the damage (e.g., delamination area) and non-discrete measurements which relate directly to structural response (e.g., compression-after-impact strength).

Discrete measurements considered in this study were the through-thickness location and extent of matrix damage, through-thickness location and extent of fiber breakage, dynamic response during impact, and surface indentation. A non-discrete measure of the damage investigated was local flexural stiffness of the damage region. The experimental technique associated with obtaining each of these responses is discussed below.

Surface Indentation. The indentation depth of all impact damage sites was measured with a dial indicator centrally mounted in a support base designed to set away from influence of the damage on flat panels. The accuracy of these readings was ± 0.025 mm.

Matrix Damage. Internal matrix damage consisted of interconnecting arrays of delaminations and transverse cracks. Ultrasonic inspections of the damage at each impact site were performed to determine the planar dimensions of matrix damage created. Additionally, the through-thickness location of matrix damage for the soft layup-thick laminate variable combination was mapped out in detail using a combination of non-destructive detailed 3-dimensionally imaged ultrasonic inspection and destructive cross-sectioning techniques. Detailed mapping of the through-thickness location of matrix damage for the three other stacking sequences (i.e., hard-thick, hard-thin, and soft thin) will be presented in the future.

Pulse-echo ultrasonics was used to locate internal delaminations by examining the amplitude and time-of-flight of a high frequency (10 MHz) short duration pulse sent into the laminate perpendicular to the surface and then received back at that surface by the same transducer. Initial investigations consisted of a coarse planar inspection of each panel to map planar location of damage created during impacting. The time-of-flight data from the overall panel scans were presented as planar (C-scan) damage maps, with various colors representing different depths of delamination.

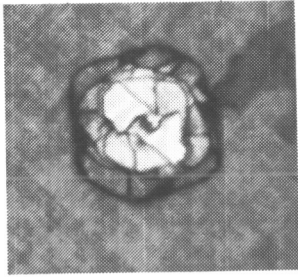
Damage sites observed in the overall panel C-scans were further investigated by performing more detailed ultrasound mappings by collecting data every 0.25 mm or 0.50 mm (depending on damage size) with a narrowly focused transducer. The damage found in these detailed scans provided information on the first levels of delamination in the laminate. Damage occurring below the first delamination encountered by a pulse at a particular point was shielded from detection because the pulse is not transmitted past that point. Planar damage area was among the data collected in these scans and was analyzed as a response below.

Two damage sites were visualized with Voxel View², a computer graphics program which allows three-dimensional viewing of volume data sets. Three-dimensional viewing helped conceptualize the extent and depth of delaminations. Data from individual through-thickness slices were plotted individually as shown in Figure 6 for panels 29-8A (soft layup-thick laminate-full experiment) and 28-2A (hard layup-thick laminate-hail simulation).

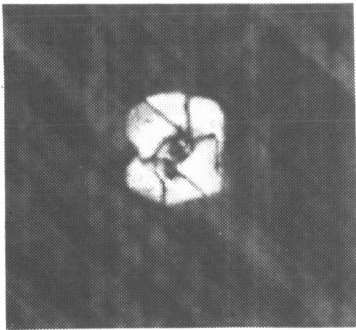
Destructive cross-section examination of an impact site from panel 29-8A was performed to determine the through-thickness location of matrix damage hidden from ultrasound inspection. The cross-section study began by waterjet cutting the impact site from the panel using the shape shown in Figure 7. The hemispherical protuberance was cut from the coupon and the edges around the circumference carefully ground down to reveal the sublaminates created by the matrix damage. Matrix damage was highlighted through the use of fluorescent-dye penetrant to aid in visual interpretation. This technique was termed cylindrical-sectioning by the authors. The sublaminate structure revealed by the cylindrical-section is shown in Figure 8. The rectangular portion was again cut 7.62 mm from the impact centerline and both these flat sections polished to further aid in interpretation of the damage state.

The accumulated matrix damage findings for panel 29-8A were summarized in schematic form as shown in Figure 9. The damage found in the vicinity of a given ply was sketched onto paper with each ply in the stack sequence represented by a sheet of paper. Transverse cracks through the ply being observed were drawn as dashed lines, the "shadow" of transverse cracks through the ply above were plotted as solid lines, and delamination between the ply being observed and the one above were represented by a shaded region. Characterization of additional impact sites in this manner will be performed in future work.

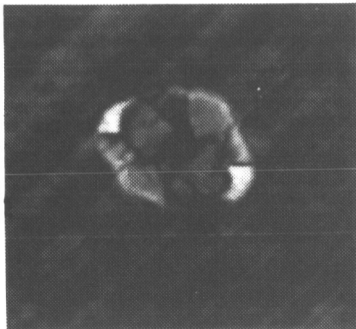
² Vital Images, Inc., 505 N. 3rd, Suite 205, Fairfield, IA, 52556.



Overall



25%

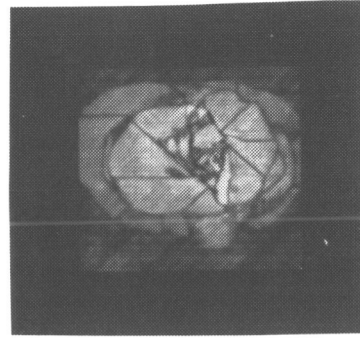


63%

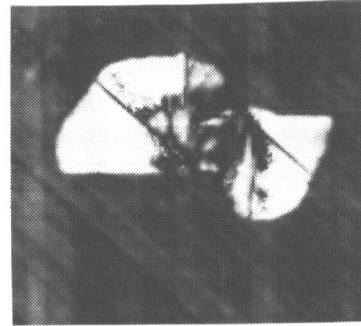


88%

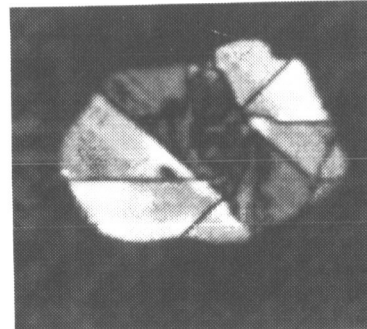
29-8A, Soft Layup



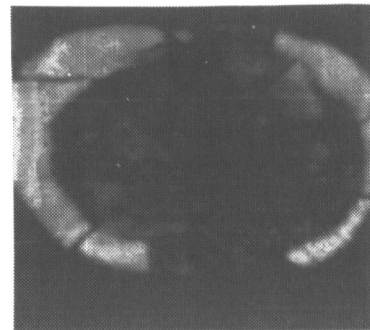
Overall



24%



34%



88%

28-2A, Hard Layup

Figure 6: Through-Thickness C-scan Images for Panels 28-2A and 29-8A.

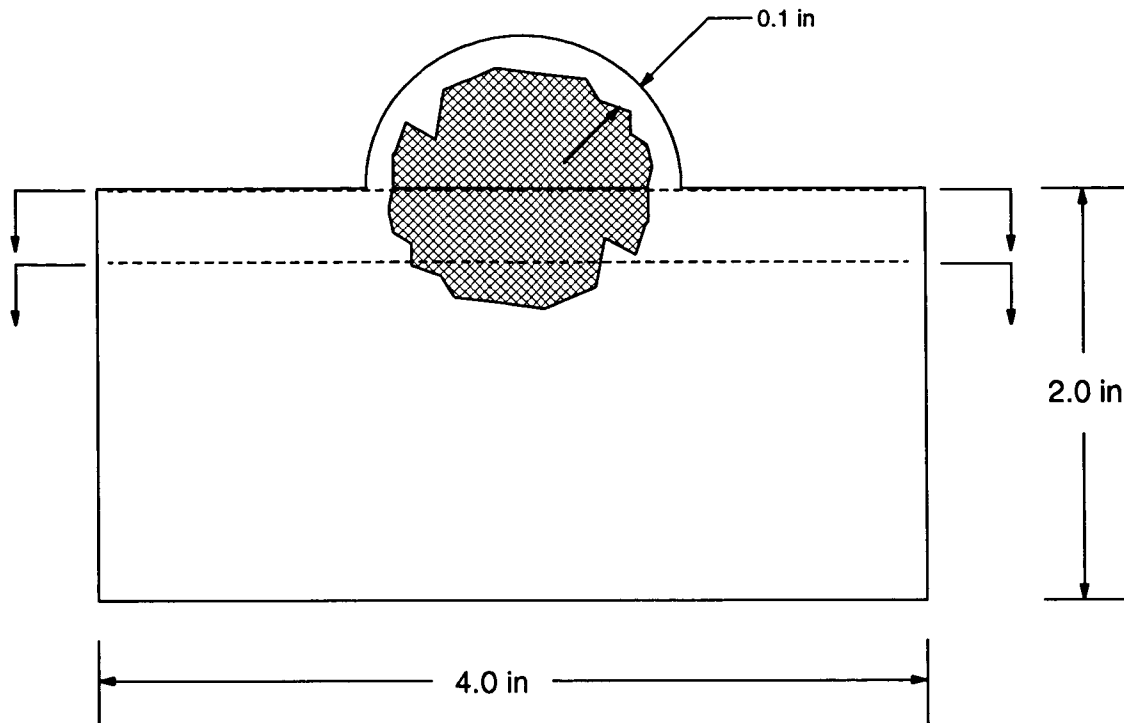


Figure 7: Cross-section and Cylindrical-section Coupon Geometry.

Mapping out the delamination planes and interconnecting transverse cracks for typical panels will provide information applicable to all panels of a given stacking sequence. The through-thickness location of matrix damage within a given stacking sequence was found in earlier studies to be chiefly a function of the stacking sequence [21]. These matrix damage maps will aid in developing an understanding of the through-thickness distribution of matrix damage as related to the intrinsic and extrinsic variables.

Fiber Failure. Fiber failures in the skin midbay impacts were measured by thermally deplying a damage site from each of the 32 panels and measuring the length of broken fibers in each ply. A numerically controlled waterjet-cutter machined 101.6 mm by 101.6 mm (4 in x 4 in) square plates with one corner cut diagonally to preserve orientation. Prior to burn-off, specimens were examined for visual damage, exact impact site location within the square, and any surface irregularities.

The deply technique consisted of placing the specimens on sheet steel shelves in a Sybron model FB1415M muffle furnace set at a temperature of 394°C to 402°C. The specimens were removed from heat after 3 hours and cooled at room temperature. Each specimen was immediately labeled and deply attempted when sufficiently cooled. If significant resin was still present, the specimen was placed back in the oven in 45 minute intervals until the resin was sufficiently burned-off.

Upon successfully deplying the first ply, each successive layer, with the impacted surface as layer one, was placed face up on a paper template imprinted with the specimen outline including orientation mark, specimen number, resin type, fiber type, stacking sequence, and date of deply. Specimens were held in place with cellophane tape placed around the periphery, taking care not to cover the impact zone.

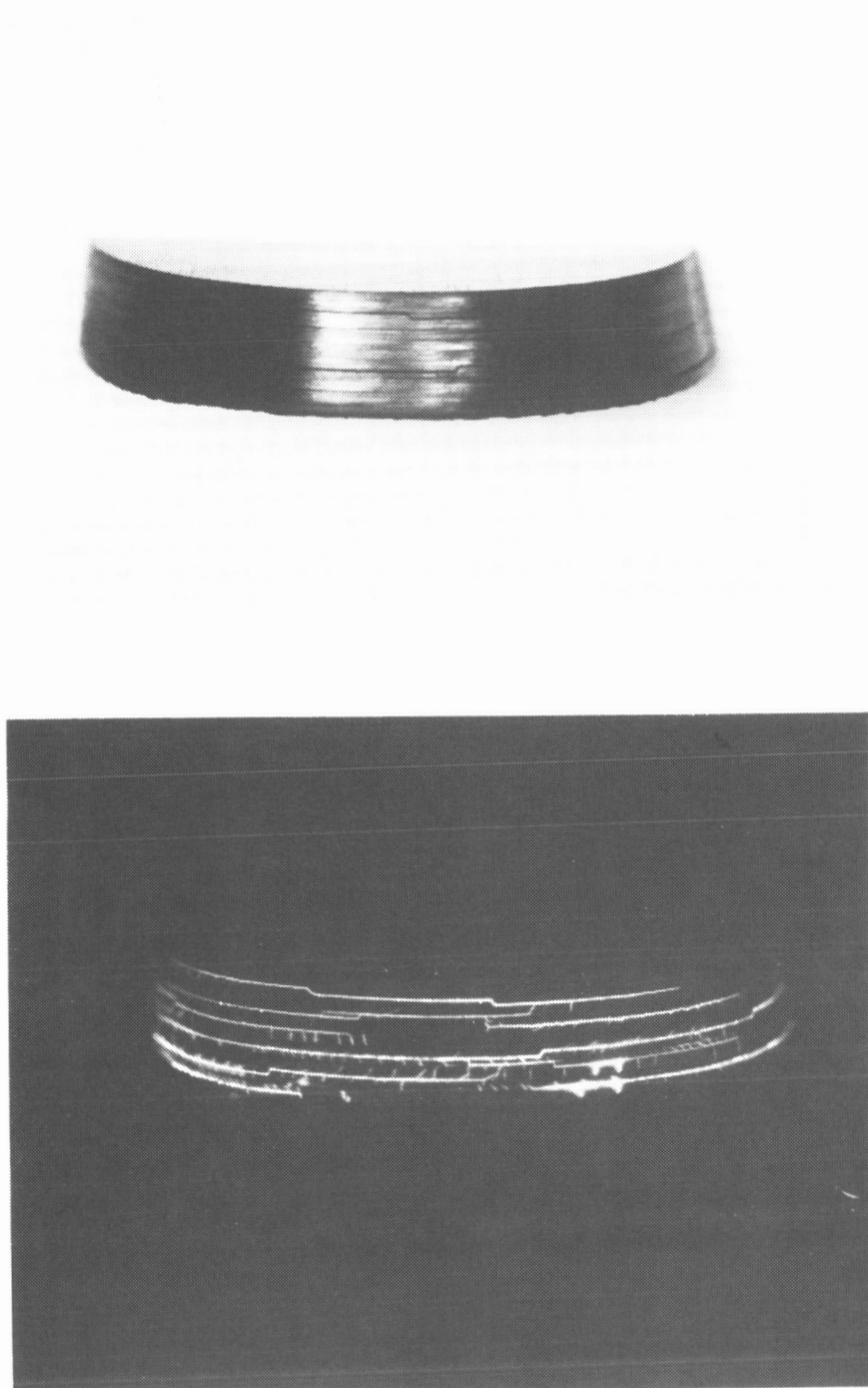


Figure 8: Cylindrical-Section Results for Panel 29-8A.

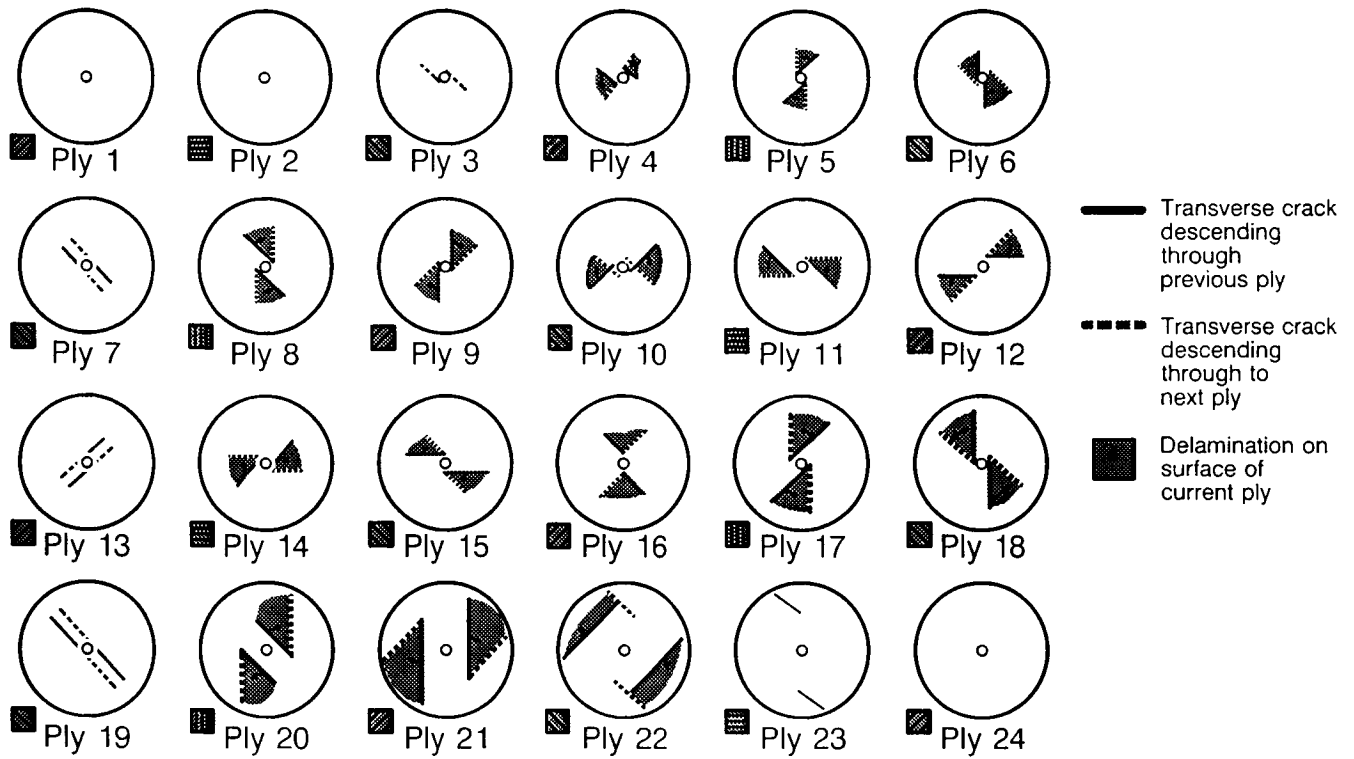


Figure 9: Ply by Ply Matrix Damage Maps for Panel 29-8A.

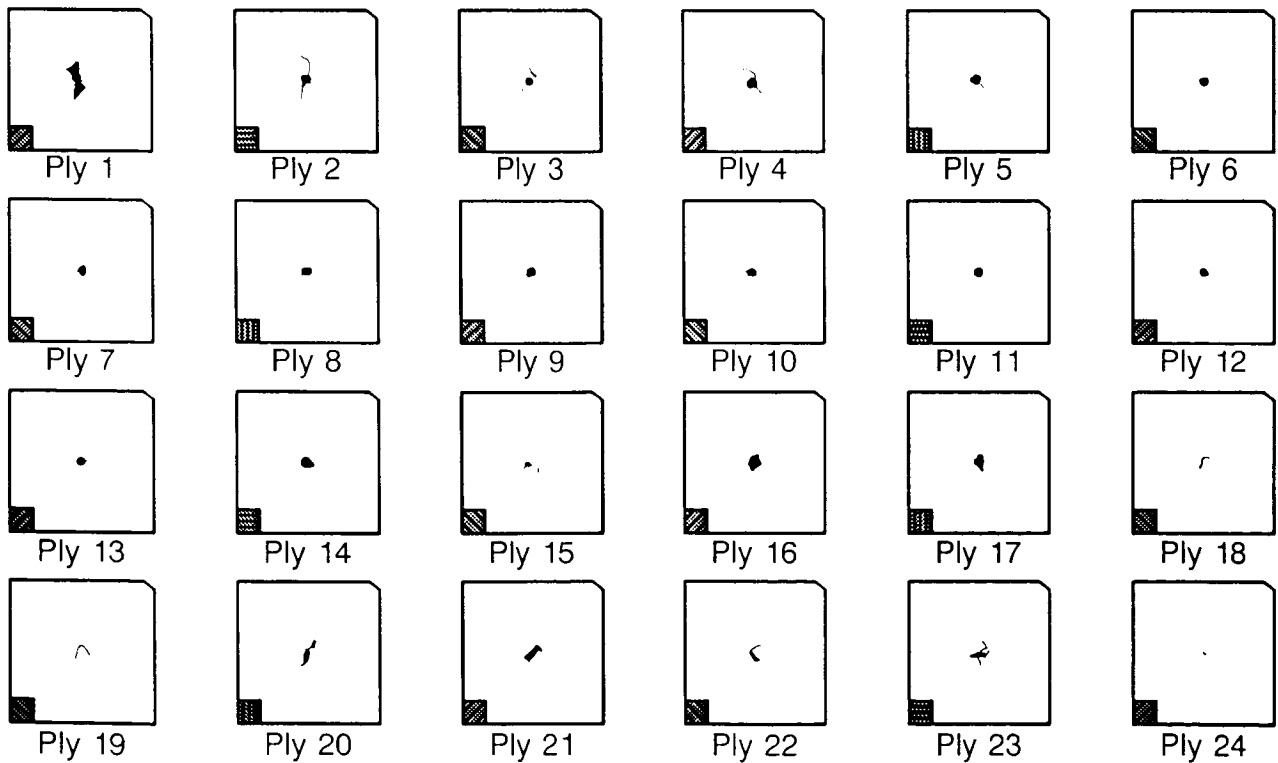


Figure 10: Ply by Ply Fiber Failure Maps for Panel 28-4A.

The length and orientation of cracks (failed fibers) in each ply were traced onto a transparency using indelible black ink. All transparencies had previously been marked with specimen outlines to maintain alignment between the transparency boundary, specimen boundary, and traced on fiber break locations. The lines of fiber breakage for each ply of panel number 28-4A are shown in Figure 10.

The data contained on the transparencies for each impact site were digitized to ease data processing. Each transparency was placed on an Apple A9M0337 scanner in a specified orientation and location and scanned into a bitmap file. The bitmap data for all plies in a specimen were transformed into a three-dimensional scientific data set and stored in Hierarchical Data Format (HDF) with a Spyglass³ utility. A utility was written to calculate the length of fiber breakage perpendicular to the fiber orientation (i.e., the length of fiber removed from the load path) in each ply. Figure 11 summarizes the fiber breakage lengths for all plies of panel number 28-4A. The slope of a best fit straight line was used to describe through-thickness distribution, although not all distributions were linear.

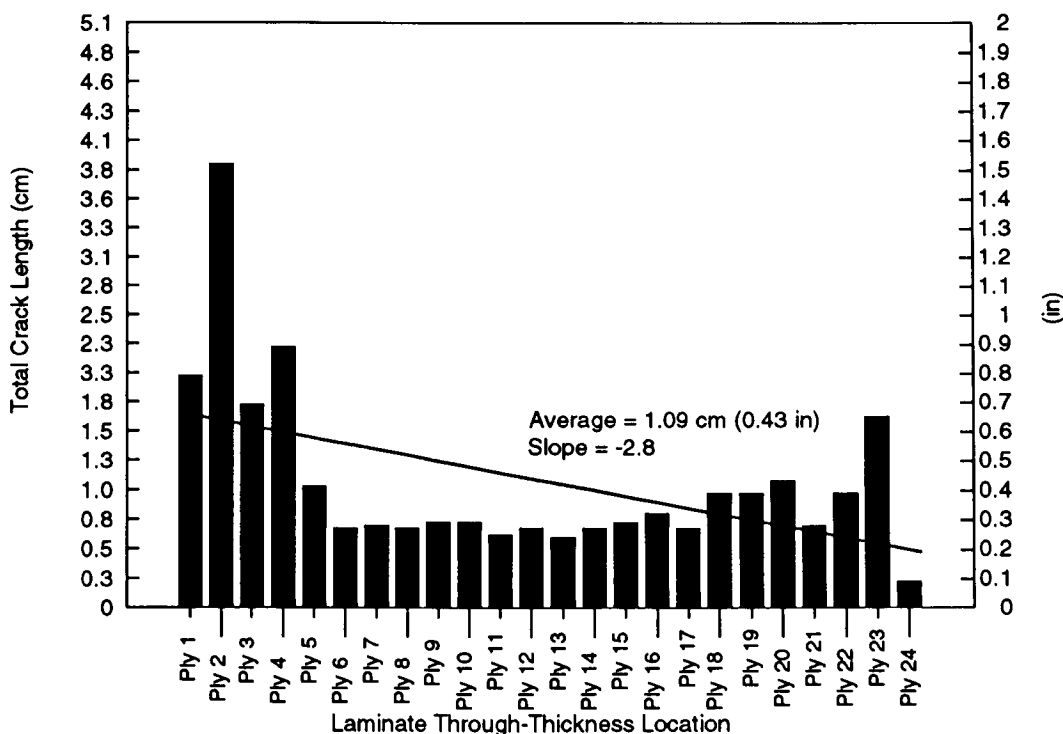


Figure 11: Summarized Fiber Failures for Panel 28-4A.

Non-discrete Measurements. A non-discrete inspection method using characteristics of flexural (Lamb) wave propagation to quantify impact damage in laminated composites was investigated. A fixture to accurately locate a sending transducer and a receiving transducer on the test panels, as shown in Figure 12, was designed and built by ZETEC of Issaquah, WA. The velocity of flexural-waves (phase velocity) propagating from the sending transducer to the receiving transducer were measured experimentally using a prototype of ZETEC's new S-9 sonicator. The measurements of phase

³ Spyglass, Inc., 701 Devonshire Dr., Champaign, IL, 61820.

velocity were made both in undamaged and damaged mid-bay regions of the panels in directions both parallel and perpendicular to the stiffeners using several excitation frequencies.

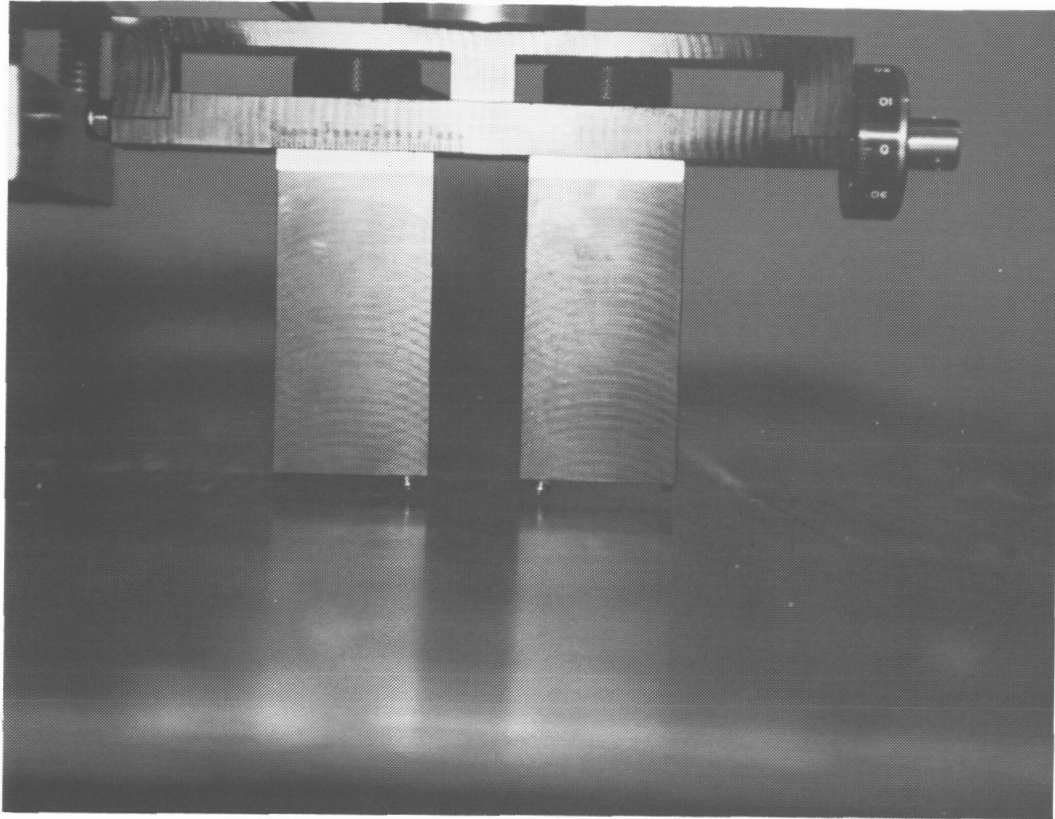


Figure 12: Apparatus for Measuring Flexural Wave Propagation through Impact Damage

RESULTS AND DISCUSSION

The full experiment and the hail simulation experiment were separate parallel studies on the same panels. These experiments were both based on the design of experiments statistical technique. The full experiment studied 14 variables (8 intrinsic and 6 extrinsic) while the hail simulation experiment studied the 8 intrinsic variables with respect to one impactor, a lead ball with 56.5 Joules of kinetic energy.

A comprehensive statistical evaluation of the experimental results which considered the complexities of these designed experiments has not yet been completed. The data analysis performed below studied the DOE results using engineering evaluation coupled with a coarse statistical analysis. The process by which the data was evaluated is described in the indentation depth discussions.

Data evaluation initially focused on studying each experiment individually to determine important effects. The results from the full and hail simulation experiments were found to complement one another and the combined study of both sets of results aided in overall data interpretation. Presentation of results and discussions of the findings will be done for each measured response using data from both experiments for justification.

Indentation depth/Visibility. Visibility of impact damage is directly related to post-impact strength requirements as illustrated in Figure 13 for commercial aircraft. The different load levels defined in this illustration are based on the amount of visible damage. Ultimate load is applicable for damage defined as nonvisible per the defined inspection technique. The Boeing Commercial Airplane Group interpretation of FAA requirements led to the definition of a 0.25 mm (0.01 in) indentation as the threshold of visibility (i.e., barely visible impact damage) based on visual inspection from 5 feet. The United States Air Force quantified the threshold for damage visibility at a 2.5 mm (0.10 inch) dent [21], based on their inspection requirements. Lower load requirements exist for structures having damage that is easily visible. The absolute levels of these loads and requirements defining them are application dependent.

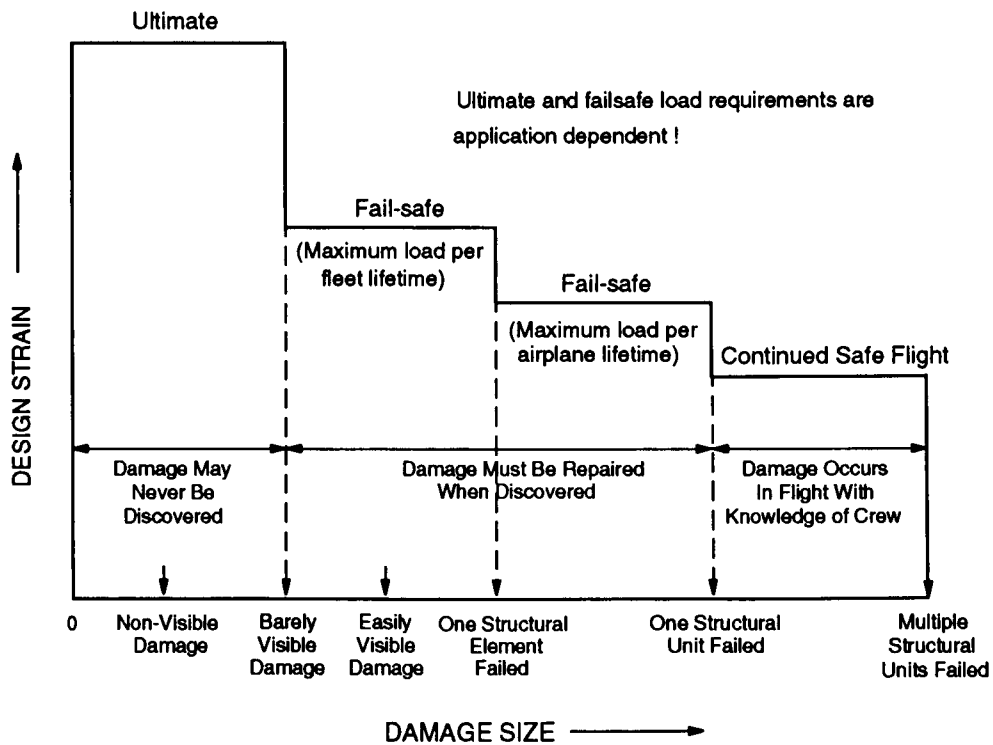


Figure 13: Structural Load Requirements as a Function of Damage Size.

Impact damage created in this study spanned the range from completely nonvisible by visual inspection to quite easily visible. Figures 14 and 15 show examples of "visible" damage (as defined by the authors inspection technique) created by simulated hail impacts. The surface indications range from a slight amount of back surface breakout (and a 0.08 mm front surface indentation) to a front surface crater larger than 2.5 mm (0.10 in) in depth.

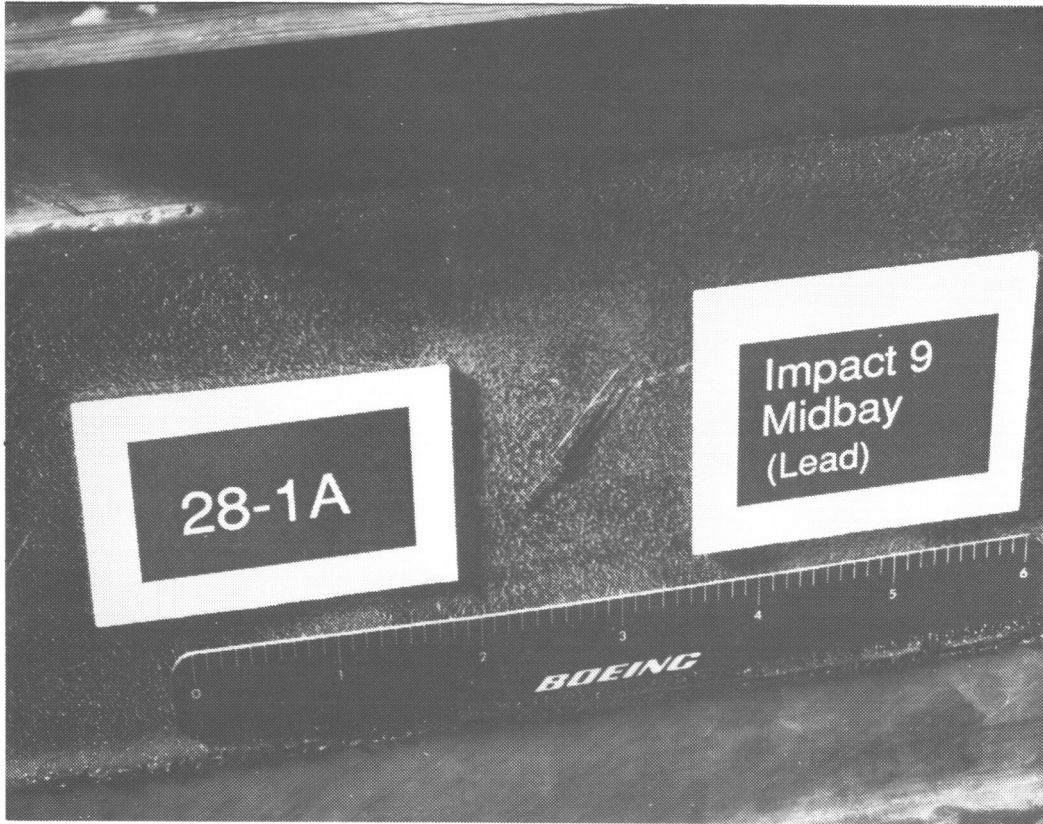


Figure 14: Barely Visible Damage.

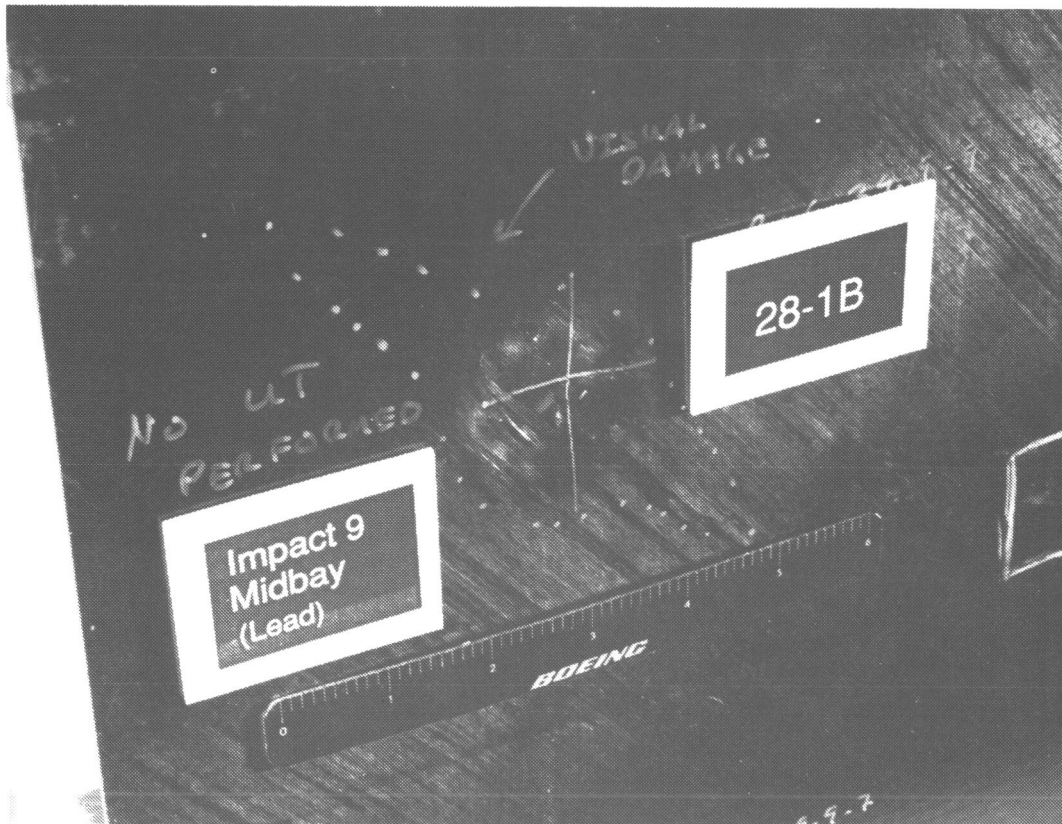


Figure 15: Clearly Visible Damage.

The indentation depth data from the hail simulation and full experiment impacts were initially evaluated using "scree plots," as defined in [18]. Scree plots displayed statistical data about each run in a histogram format to identify potentially important variables and variable interactions. The average response for each substantial variable or variable interaction was calculated to determine its effect (on indentation). Those with large effects compared to the majority of measured effects were considered important.

Figure 16 illustrates effect calculation for the "Laminate thickness" variable using hail simulation data. The measured indentation depth is represented on the y-axis and the run numbers, as defined in Table 3, are along the x-axis. Each vertical bar represents the indentation depth for the listed run number. These data were grouped into two halves, runs with thin laminate panels and runs with thick laminate panels. The average level of each half was calculated, and the difference between the two halves divided by 2 to estimate the effect.

Two-factor interactions were evaluated in a similar manner, as illustrated in Figure 17 for the "Fiber type-Fiber volume" interaction. The data were first grouped according to "Fiber type." Within each "Fiber type" group the data were sub-grouped according to "Fiber volume," and the average level for each quarter of the runs, as defined by these divisions, was calculated. The sum of the average level for the AS4, 56% fiber volume (FV) group and the IM7, 48% FV subgroup was subtracted from the sum of the average level for the AS4, 48% FV subgroup and the IM7, 56% FV. The resulting value was divided by 4 to obtain an estimate of the effect of this interaction.

Half the data in the AS4, 48% FV subgroup were observed to be higher than the rest. These runs were studied to determine if one variable could account for the differences, and "Laminate thickness" was found to correlate with the observed variations. Bars representing data from runs with thin laminate panels were crosshatch shaded, while runs from thick laminate panels were solid shaded. It is apparent in Figure 17 that the high values in this subgroup are all thin laminate panels, suggesting that a three-way interaction between "Laminate thickness"-"Fiber type"-"Fiber volume" may exist.

Two factor interactions such as the one illustrated in Figure 17 are often confounded with other two factor interactions. The patterns and levels of confounding were defined by the method of statistical experimental design and number of variables studied [18, 19]. The design of this experiment resulted in the "Fiber type-Fiber volume" interaction being confounded with the "Matrix type-Material form" interaction shown in Figure 18 and the "Skin layup-Stiffener type" interaction (not shown). Statistically, the estimated effect for this set of three potential interactions is the sum of the estimated effects for these interactions, and is not separable. Engineering judgement and/or further experimentation must be used to sort out the true significant interactions.

Deduction of some confounded interactions was accomplished by the examination of results from both experiments. An example of this process is illustrated with the aid of Table 5. Listed are the confounded interactions that made up the second most important effect for indentation depth in both experiments. The first three potential interactions listed are identical for the two experiments; therefore, one can hypothesize that it is unlikely that interactions 4 through 6 of the full experiment are significant, since they do not occur in the hail simulation experiment. The "Skin layup-Stiffener type" interaction is improbable because "Stiffener type" relates to the stiffness of the panel during impact, and should not interact with "Skin layup." The most likely candidates for the actual interaction are "Fiber type-Fiber volume" or "Matrix type-Material form".

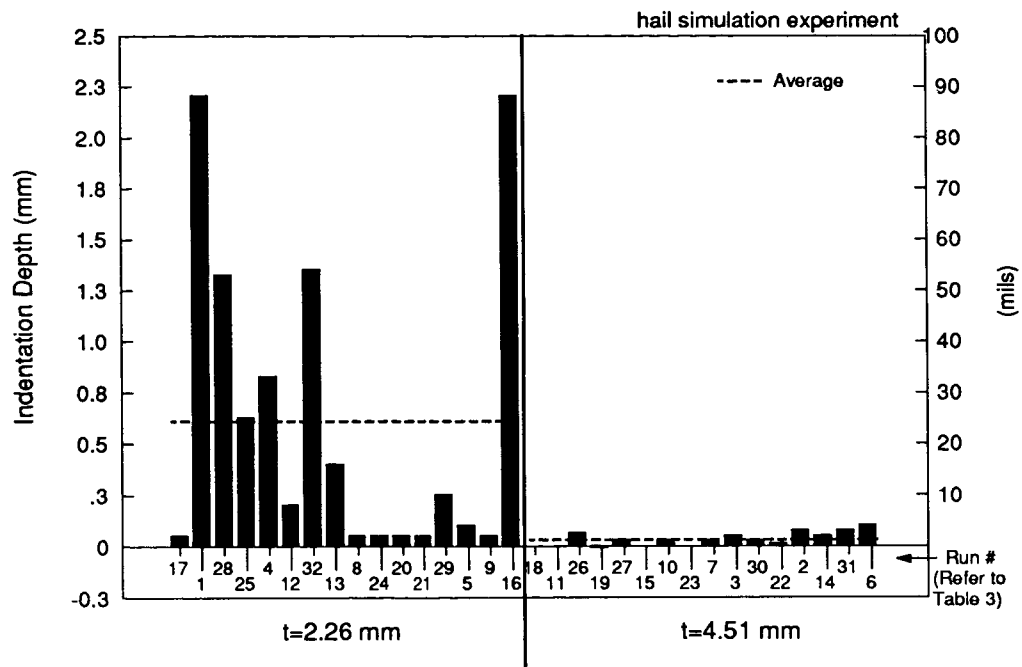


Figure 16: Laminate thickness Effect for Hail Simulation Experiment Indentation Depth

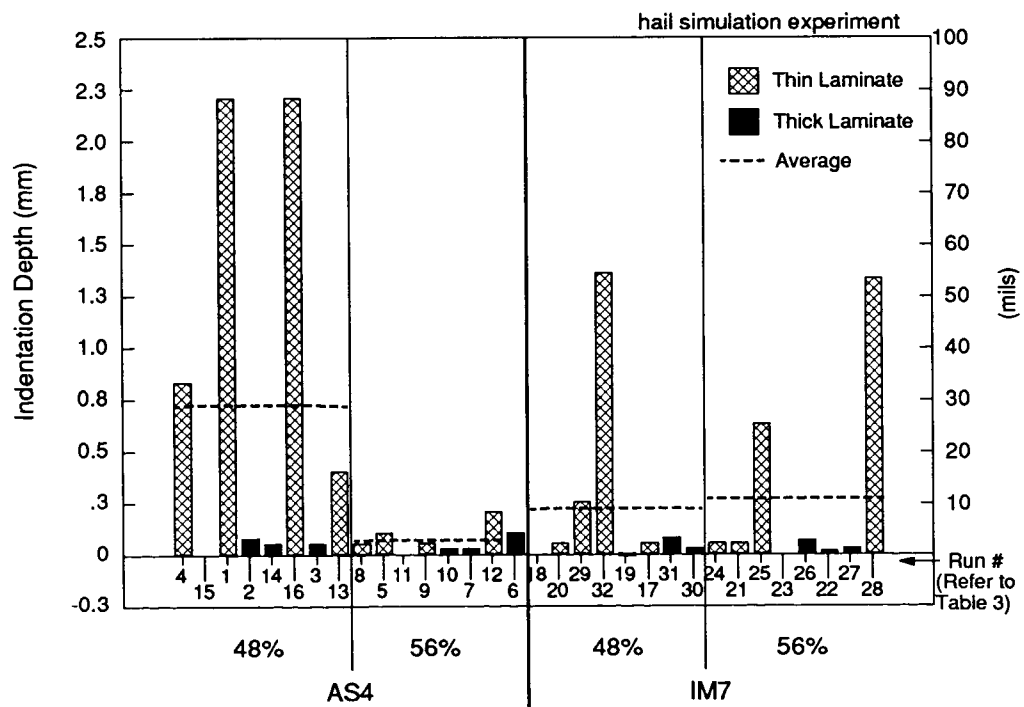


Figure 17: Fiber type-Fiber volume Interaction for Hail Simulation Experiment Indentation Depth.

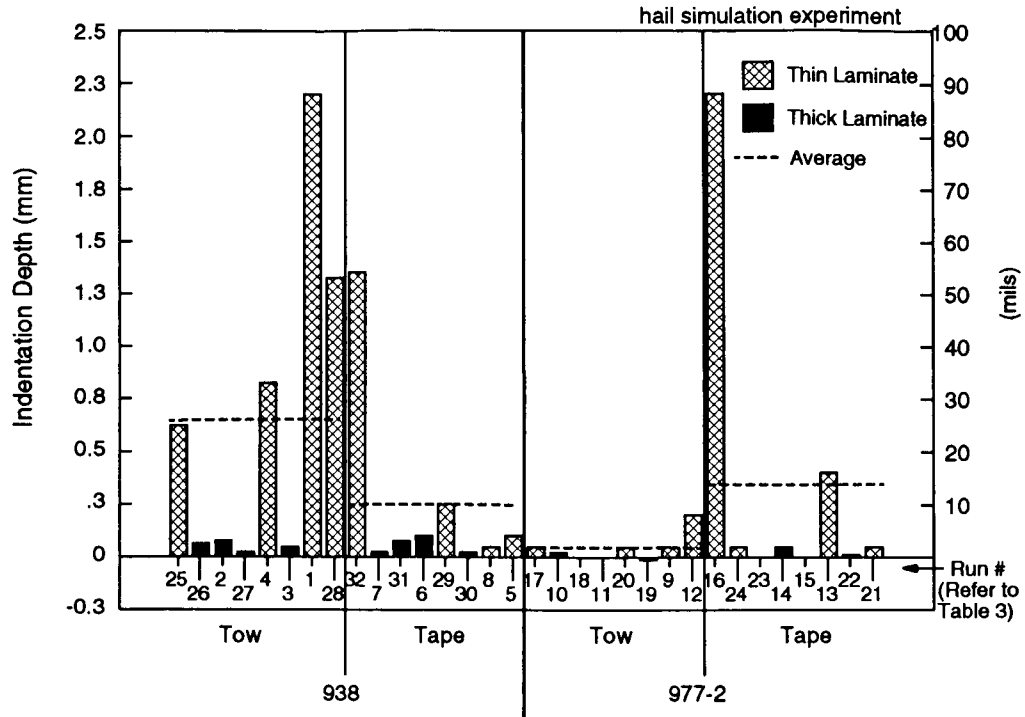


Figure 18: Matrix type-Material form Interaction for Hail Simulation Experiment Indentation Depth.

Full Experiment	Hail Simulation
1) Fiber type-Fiber volume 2) Matrix type-Material form 3) Skin layup Stiffener type 4) Impactor stiffness Stiffener spacing 5) Laminate thickness Impact energy 6) Impactor shape Temperature	1) Fiber type-Fiber volume 2) Matrix type-Material form 3) Skin layup Stiffener type

Table 5: Interaction Deduction for the Indentation Depth Response

A summary of the most important variables (main effects) and variable interactions (interaction effects) as related to indentation depth from both the hail simulation and the full experiment is listed in Table 6. These effects are ranked according to their importance based on the full experiment. Interactions were listed below the main effects for clarity, and not to suggest a lesser importance of the effect. Ranking of important variables identified in the hail simulation experiments are shown in parentheses.

Rank	Variable	Low Level	High Level	Result
1	Impact energy	23 Joules	136 Joules	Increased
3	Impactor diameter	6.35 mm	25.4 mm	Decreased
4	Impactor shape	Flat	Spherical	Increased
11 (1)	Laminate thickness	2.26 mm	4.51 mm	Decreased
Important Interactions				
2 (2)	Fiber type-Fiber volume or Matrix type-Material form			

Note: Ranking of hail simulation results shown in parentheses.

Table 6: Important Effects for the Indentation Depth Response.

Impact energy was found to be the most important variable influencing indentation depth for the full experiment, as might be expected. The second most important effect was the set of confounded interactions discussed previously. Variables associated with impactor geometry were found to have a pronounced effect on the observed indentations, while laminate thickness was most important when all other impactor variables were ignored.

The strong influence of impactor geometry on indentation comes as no surprise. The relative importance of these variables on the results suggests that attempting to relate surface indentation to the internal damage state or residual strength to be a formidable task. The load requirements, as illustrated in Figure 13, are a strong function of the "visibility;" therefore, studies on impact must consider the wide range of potential threats at all realistically possible impact energies to determine worst case scenarios for each load requirement.

Matrix Damage. Measurements of planar damage area as determined from ultrasonic inspection were studied using the designed experiment. The results summarized in Table 7 were found to have the most important effects, with the ranking based on importance determined in the full experiment. Ranking of important effects from the hail simulation experiment are labeled with parentheses. Three-dimensional characterization of the sublaminar structure which relates directly to the compression after impact strength [2, 22] was attempted but has not yet been completed for all runs. The study of the data using the designed experiment required a completed data set.

Impact energy was found to be the most important variable effecting planar damage area, as expected. Following this was the set of six confounded interactions. Impactor diameter was found to have a stronger effect than the matrix type, with large diameter impactors creating larger damage areas. Higher interlaminar toughness of the matrix tended to restrict the damage size, but an examination of the "Matrix type-Laminate thickness" interaction for both the hail simulation and full experiments, shown in Figures 19 and 20, respectively, indicates that effect of toughness was most notable for thick laminates.

Rank	Variable	Low Level	High Level	Result
1	Impact energy	23 Joules	136 Joules	Increased
3	Impactor diameter	6.35 mm	25.4 mm	Increased
4 (2)	Matrix type	938	977-2	Decreased

Important Interactions	
6 (1)	Matrix type-Laminate thickness
2	Impact energy-Impactor diameter or Impactor mass-Temperature at impact or Fiber volume-Impactor stiffness or Fiber type Stiffener spacing or Matrix type Stiffener type or Material form Skin layup
5 (3)	Fiber volume-Laminate thickness

Note: Ranking of hail simulation results shown in parentheses.

Table 7: Important Effects for the Planar Damage Area Response.

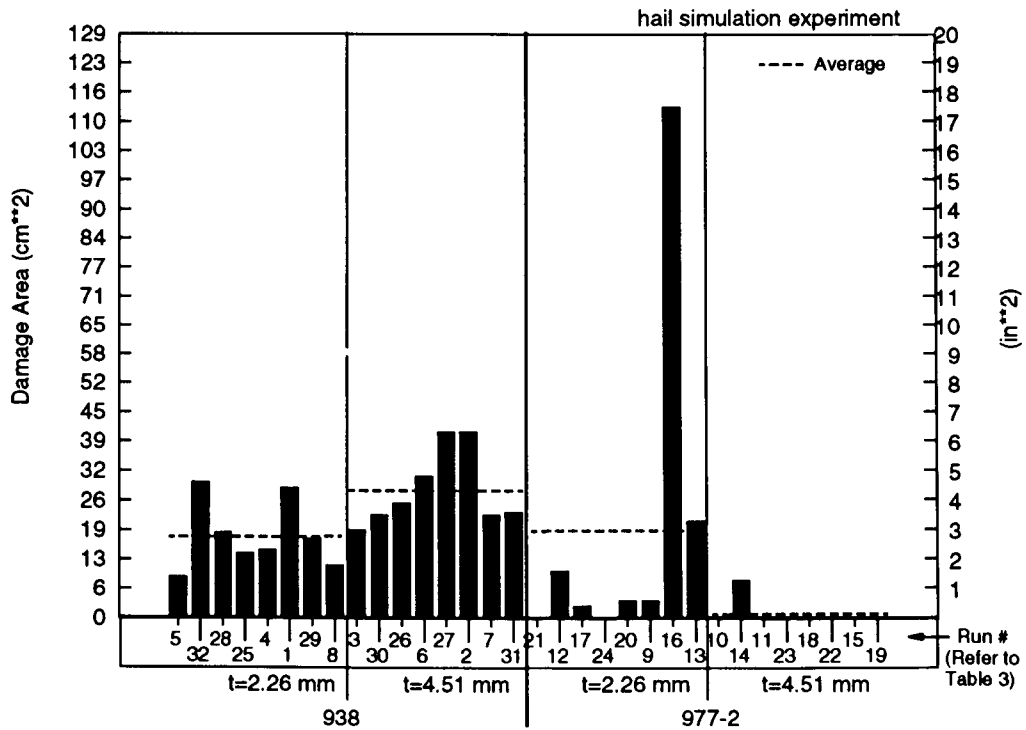


Figure 19: Matrix type-Laminate thickness Interaction for Hail Simulation Experiment Planar Damage Area.

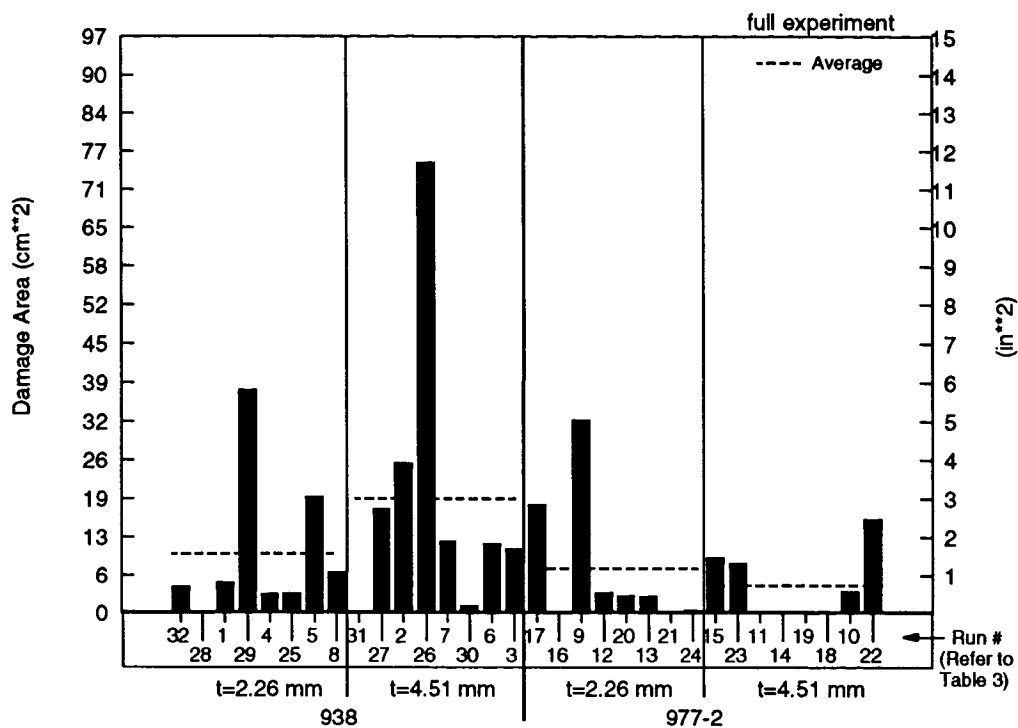


Figure 20: Matrix type-Laminate thickness Interaction for Full Experiment Planar Damage Area.

The set of six interactions, ranked 2 in Table 7, only appeared in the full experiment. "Fiber type-Stiffener spacing," "Matrix type-Stiffener type," and "Material form-Skin Layup" are interactions which do not involve impactor variables and are therefore unlikely. "Impact energy-Impactor diameter" is thought to be the likely interaction of the remaining three, because "Impactor diameter" was found to have a strong effect. Figure 21 illustrates this interaction. The average damage area for the low impact energy appears insensitive to impactor diameter, but damage area increases significantly with impactor diameter for higher levels of impact energy. The occurrence of fiber failures and subsequent perforation may explain these observations, illustrating the failure mechanism interplay between fiber and matrix damage during impact.

Planar damage areas in the hail simulation experiment were strongly influenced by a "Fiber volume-Laminate thickness" interaction. The thin laminates with high fiber volumes were found to have smaller damage areas than thin laminates with a low fiber volume. Damage areas in the thick laminate panels were not significantly influenced by fiber volume for this experiment, although the full experiment and past internal Boeing studies have found that decreased fiber volume decreased damage area for thicker laminates. This trend may have been obscured in the hail simulation by the range of variables studied.

Fiber Failure. Impact induced fiber failures were quantified both by their average length and through-thickness distribution for the full experiment impacts. The data on broken fibers may further be quantified in terms of their effect on the local load paths and strength as discussed in [3, 4, and 23], but has not yet been attempted. Table 8 lists the important observations for the fiber failure average length response.

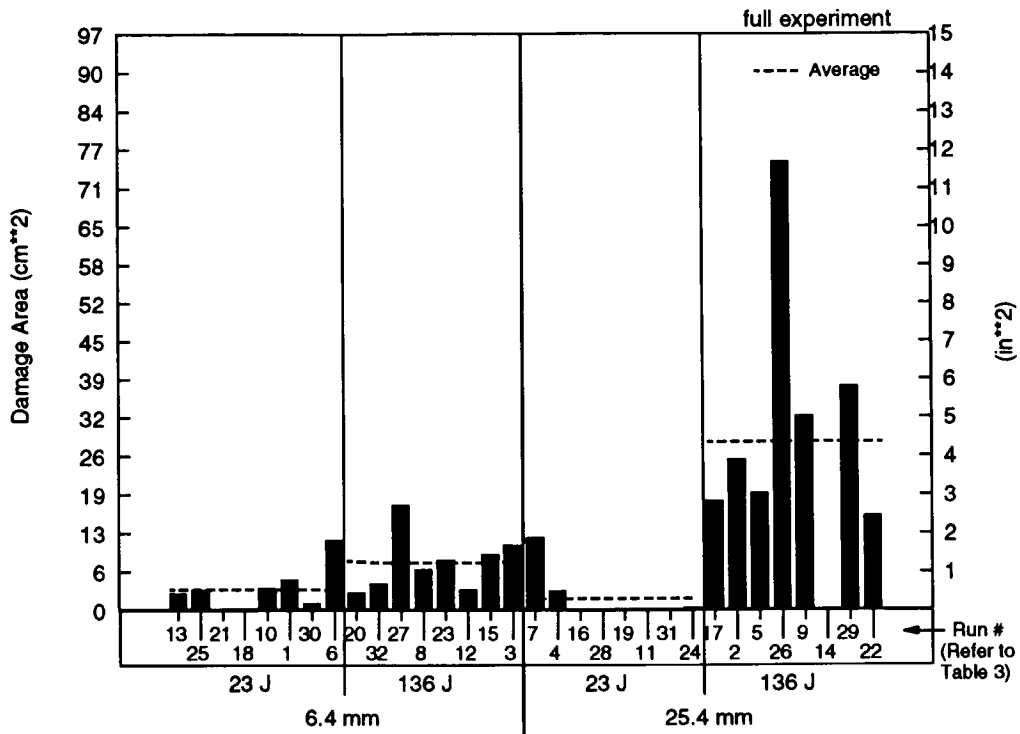


Figure 21: Impactor diameter-Impact energy Interaction for Full Experiment Planar Damage Area.

Rank	Variable	Low Level	High Level	Result
1	Impact energy	23 Joules	136 Joules	Increased
3	Laminate thickness	2.26 mm	4.51 mm	Decreased
4	Impactor diameter	6.35 mm	25.4 mm	Increased
5	Impactor shape	Flat	Spherical	Increased

Important Interactions	
2	Impactor diameter-Impact energy or Impactor mass-Temperature at impact or Fiber volume-Impactor stiffness or Fiber type-Stiffener spacing or Matrix type-Stiffener type or Material form-Skin layup

Table 8: Important Effects for the Fiber Failure Average Length Response.

Impact energy was again found to be the strongest variable, with higher energies leading to more fiber failure. Second was a set of confounded two-factor interactions. Interaction deduction was not aided by results from the hail simulation experiment because fiber failure data was not collected. Increasing the laminate thickness tended to decrease the amount of fiber failure while an increase was found for the larger impactor diameters. Spherical impactors generally created more fiber failure than the flat impactors because of higher contact pressures.

The "Impactor diameter-Impact energy" interaction is illustrated in Figure 22. Although the six interactions are statistically confounded, common sense evaluation led the authors to believe this to be the most likely of these two-factor interactions. The contact pressures, and hence local fiber breaks, were larger for the 6.35 mm (0.25 in) diameter impactor for energies below the perforation threshold, while large diameter impactors created more fiber failure at high impact energies which caused perforation.

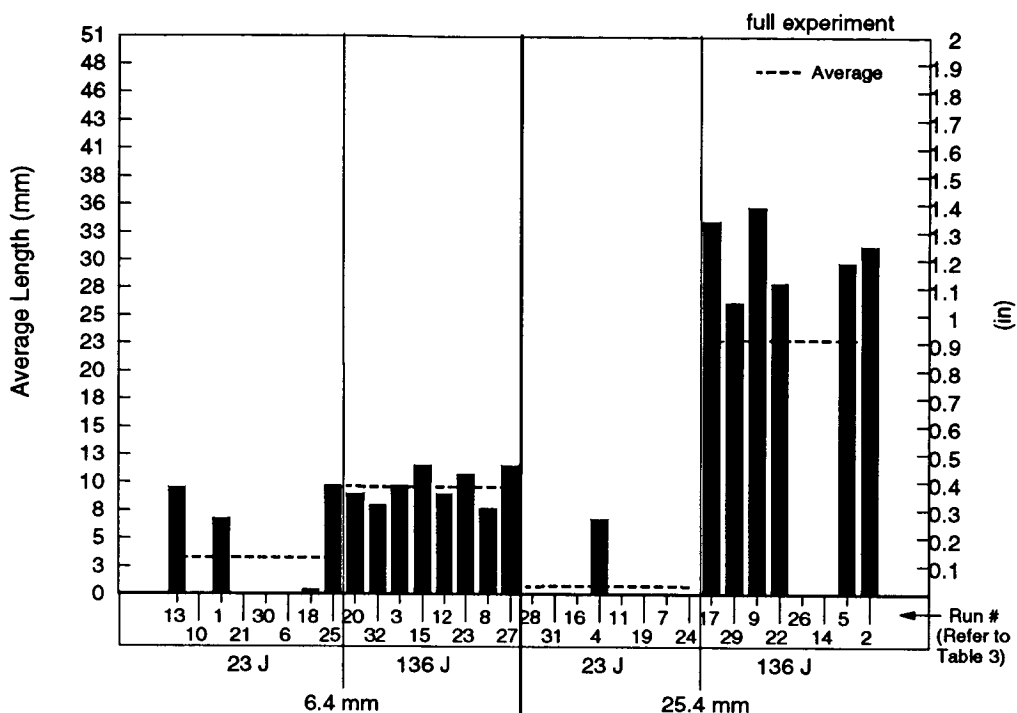


Figure 22: Impact diameter-Impact energy Interaction for Full Experiment Fiber Failure Average Length.

Results for through-thickness distribution of fiber failures are listed in Table 9. Although these results have not yet been studied in detail, it is of interest that the material form may influence the damage state. Thinner laminates tended to have a more uniform fiber breakage distribution, while higher impact energies decreased the uniformity. A two-way interaction is again among the important effects.

Non-discrete Measurements. The reduction in compression strength of laminated composites has been attributed to the buckling of sublaminates created by impact induced matrix damage followed by local load redistribution [2]. Sublaminates buckling is directly related to the flexural stiffnesses of these sublaminates. Flexural wave propagation in a plate is also a function of the bending and shear stiffnesses. It was theorized that the presence of impact damage would result in reduced flexural wave speeds, allowing both detection of the damage and assessment of the associated stiffness reduction.

Dispersion curves, which relate phase velocity to frequency, were generated for the undamaged laminates using the theoretical formulation found in [24]. This formulation was based on laminated plate theory and included the effects of shear deformation and rotary inertia. Experimental measurements of phase velocity as a function of frequency for undamaged regions of the panels were compared to the theory for mutual verification. Measurements and comparisons were made both 0° and 90° to the stiffeners because the phase velocity in a composite laminate is dependent on the direction of propagation due to material anisotropy.

The measured phase velocities in the undamaged regions agreed well with theoretical predictions. Phase velocities in damaged regions were less than those in the undamaged regions as theorized. Figure 23 shows the comparison between theory and experiment for the undamaged laminate along with data from the damaged region. Damage sites with extreme amounts of damage proved difficult to measure experimentally with the current techniques. This difficulty was probably caused by excessive attenuation of the signal and by waves reflected from the damage boundary.

Rank	Variable	Low Level	High Level	Result
1	Laminate thickness	2.26 mm	4.51 mm	Decreased
2	Material form	Tow	Tape	Decreased
3	Impact energy	23 Joules	136 Joules	Increased

Important Interactions	
4	Fiber type-Impactor mass or Matrix type-Laminate thickness or Material form-Impact energy or Layup-Impactor diameter or Impactor stiffness-Impactor shape or Stiffener spacing-Temperature

Table 9: Important Effects for the Fiber Failure Through-Thickness Distribution Response.

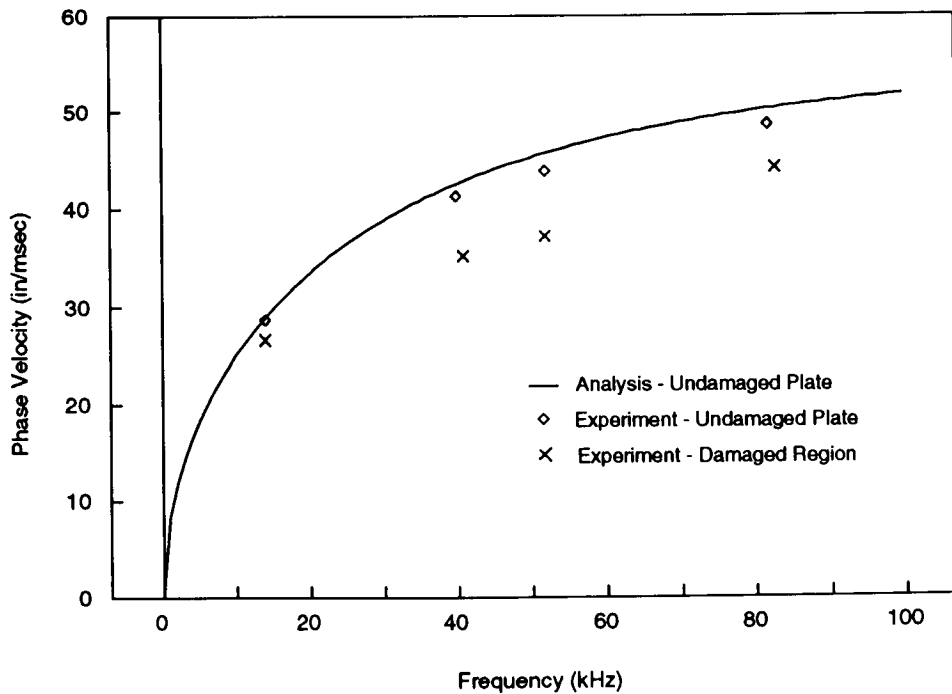


Figure 23: Theoretical Dispersion Curve and Experimentally Measured Data for Panel 28-6A

CONCLUSIONS

This experiment resulted in a relative ranking of the important variables and variable interactions studied. Variables found to have little effect are not necessarily unimportant, but were overshadowed by the effects of others. Future studies on impact should consider the important variables and interactions. These results are meant to guide future studies, and are not the final judgement. The important findings are summarized below.

Impact energy and impactor geometry were the chief extrinsic variables affecting both internal damage and surface visibility. Important variables associated with impactor geometry were the diameter and shape. Larger diameter impactors were found to create more damage (impact energy not being held constant) and less surface indication, while impact energy had direct correspondence to the damage state and external indications. The strong couplings between these extrinsic impact variables and damage characteristics suggest the need for a more comprehensive material and design screening approach.

Intrinsic material variables were generally less important than extrinsic variables when considering the range of variables and variable levels studied in the full experiment. Matrix toughness appeared to have little effect on impact damage in minimum gauge structure (i.e., 0.09 in thick), which is characteristic of 70% of fuselage shell, but did reduce the damage in thicker fuselage skin gauges characteristic of compression loaded keel structures. Fiber type, by itself, was found to have little effect on impact damage.

Interactions between variables were found to have a stronger influence on the damage state than most variables by themselves. These two- and possibly three- factor interactions must be better understood and accounted for in future impact studies. An understanding of important interactions between laminate and material variables may lead to breakthroughs in damage resistant composite design.

Laminate thickness was the critical design variable when considering the indentation created by simulated hail impacts. Economic considerations on hail induced damage have led to minimum fuselage gauge requirements to avoid frequent repairs. Increased laminate thickness reduced indentation/visibility of damage created by hail impact, while higher fiber volumes reduced internal damage for the thin gauge laminates. Efficient hail damage resistant structure should result from further study and understanding of these effects.

Ultrasonic Lamb wave propagation has potential as a quantitative method of characterizing impact damage in fuselage structure. Experimental results were within 5% of theory for undamaged laminate measurements and demonstrated the expected trends for measurements of the damage.

ACKNOWLEDGMENTS

The authors wish to acknowledge G. Cox, S. Finn, R. Horton, J. Linn, W. Motzer, L. Nuanez, P. Puzon, P. Smith, K. Willden, and M. Wood of The Boeing Company; T. Brown and C. Grant of Hercules, Inc.; R. Wishart of Integrated Technologies, Inc.; R. Bennett, D. Delfosse, A. Poursartip, G. Pageau, and R. Vaziri of the University of British Columbia; and R. Groh and D. Newkirk of the University of Washington for technical support.

NOTICE

Use of commercial products or names of manufacturers in this report does not constitute official endorsement of such products or manufacturers, either expressed or implied, by The Boeing Company or The National Aeronautics and Space Administration.

REFERENCES

1. Rhodes, M. D., Williams, J. G., and Starnes, J. H. Jr., "Effect of Impact Damage on the Compression Strength of Filamentary-Composite Hat-Stiffened Panels," Society for the Advancement of Material and Process Engineering, Vol. 23, May 1978.
2. Dost, E. F., Ilcewicz, L. B., and Gosse, J. H., in Proc. of 3rd Tech. Conf. of American Soc. for Composites, Technomic Publ. Co., 1988.
3. Cantwell, W. J., Curtis, P. T., and Morton, J., "An Assessment of the Impact Performance of CFRP Reinforced with High Strain Carbon Fibres," Composite Science and Technology, Vol. 25, 1986.
4. Cairns, D. S. and Lagace P. A., "Residual Tensile Strength of Graphite/Epoxy and Kevlar/Epoxy Laminates with Impact Damage," Massachusetts Institute of Technology, TELAC Report 88-3, 1988.
5. Rhodes, M. D., Williams, J. G., and Starnes, J. H. Jr., "Low-Velocity Impact Damage in Graphite-Fiber Reinforced Epoxy Laminates," Proceedings of the 34th Annual Technical Conference of the Reinforced Plastics/Composite Institute, The Society of the Plastics Industry, Inc., 1979.
6. Byers, B. A., "Behavior of Damaged Graphite/Epoxy Laminates Under Compression Loading," NASA Contractor Report 159293, 1980.
7. Smith, P. J. and Wilson, R. D., "Damage Tolerant Composite Wing Panels for Transport Aircraft," NASA Contractor Report 3951, 1985.
8. Chapman, A. J., "Standard Test Evaluation of Graphite Fiber/Resin Matrix Composite Materials for Improved Toughness," NASA Technical Memorandum 86298, 1984.
9. Palmer, R. J., "Investigation of the Effect of Resin Material on Impact Damage to Graphite/Epoxy Composites," NASA Contractor Report 165677, 1981.
10. Masters, J. E., "Characterization of Impact Damage Development in Graphite/Epoxy Laminates," Fractography of Modern Engineering Materials: Composites and Metals, ASTM STP 948, ASTM, Philadelphia, PA, 1987.
11. Evans, R. E., and Masters, J. E., "A New Generation of Epoxy Composites for Primary Structural Applications: Materials and Mechanics," Toughened Composites, ASTM STP 937, ASTM, Philadelphia, PA, 1987.
12. Dow, M. B. and Smith, D. L., "Damage-Tolerant Composite Materials Produced by Stitching Carbon Fabrics," International SAMPE Technical Conference Series, Volume 21, 1989.
13. Palmer, R. J., Dow, M. B., and Smith, D. L., "Development of Stitching Reinforcement for Transport Wing Panels," NASA Conference Publication 3104, 1990.
14. Ko, F. K. and Hartman, D., "Impact Behavior of 2D and 3D Glass-Epoxy Composites," SAMPE Journal, July/Aug 1986.
15. Boll, D. J., Bascom, W. D., Weidner, W.C., and Murri, W.J., "A Microscopic Study of Impact Damage of Epoxy-Matrix Carbon-Fibre Composites," Journal of Material Science, Vol 21, 1986.

16. Swanson, G. D., Ilcewicz, L. B., Walker, T. H., Graesser, D., Tuttle, M., and Zabinski, Z., "Local Design Optimization for Transport Fuselage Crown Panels," in Proceedings of Ninth DoD/NASA/FAA Conference on Fibrous Composites in Structural Design, FAA Publication, 1991.(Paper of this compilation.)
17. Joynes, D., "Inservice Experience and Maintenance of Advanced Composite Structures in Airline Service," International SAMPE Technical Conference Series, Volume 22 ,1990.
18. Wheeler, D. J., Understanding Industrial Experimentation, Statistical Process Controls, Inc., Knoxville, TN, 1988.
19. Wheeler, D. J., Tables of Screening Designs, Second Edition, SPC Press, Inc., Knoxville, TN, 1989.
20. Chamis, C. C., "Simplified Composite Micromechanics Equations for Hygral, Thermal, and Mechanical Properties," NASA TM-83320, National Aeronautics and Space Administration, Feb., 1983.
21. Horton, R., Whitehead, R., et al, "Damage Tolerance of Composites, Final Report," AFWAL-TR-87-3030, Vol. 3, May 1988.
22. Dost, E. F., Ilcewicz, L. B., and Avery, W. B., "The Effects of Stacking Sequence On Impact Damage Resistance and Residual Strength for Quasi-Isotropic Laminates," in Composite Materials: Fatigue and Fracture, ASTM STP 1110, 1991.
23. Walker, T. H., Avery, W. B., Ilcewicz, L. B., Poe, C. C., Jr., and Harris, C. E., "Tension Fracture of Laminates for Transport Fuselage, Part I: Material Screening," in Proceedings of Ninth DoD/NASA/FAA Conference on Fibrous Composites in Structural Design, FAA Publication, 1991.(Paper of this compilation.)
24. Tang, B., Henneke, E. G., and Stiffler, R. C., "Low Frequency Flexural Wave Propagation in Laminated Composite Plates," published in the Proceedings of Acousto-Ultrasonics: Theory and Application, 1988.